University of Iowa

Iowa Research Online

Theses and Dissertations

Fall 2009

Effect of chamber pressure on liquid drop impacts on a stationary smooth and dry surface

Neeraj Kumar Mishra
University of Iowa

Recommended Citation
Mishra, Neeraj Kumar. "Effect of chamber pressure on liquid drop impacts on a stationary smooth and dry surface." MS (Master of Science) thesis, University of Iowa, 2009.
https://doi.org/10.17077/etd.7x54zfin

EFFECT OF CHAMBER PRESSURE ON LIQUID DROP IMPACTS ON A

STATIONARY SMOOTH AND DRY SURFACE

by

Neeraj Kumar Mishra

A thesis submitted in partial fulfillment of the
requirements for the Master of Science degree in
Mechanical Engineering in the Graduate College of
The University of Iowa

December 2009

Thesis Supervisor: Assistant Professor Albert Ratner

Graduate College
The University of Iowa
Iowa City, Iowa

CERTIFICATE OF APPROVAL
_____

MASTER'S THESIS
_____

This is to certify that the Master's thesis of

Neeraj Kumar Mishra

has been approved by the Examining Committee for the thesis requirement for the
Master of Science degree in Mechanical Engineering at the December 2009
graduation.

Thesis Committee: _____
                    Albert Ratner, Thesis Supervisor

                  _____
                    Ching-Long Lin

                  _____
                    James H. Buchholz

ACKNOWLEDGEMENTS

I would like to thank the Graduate College, University of Iowa, for giving me this chance to pursue a Master's degree at this university. Many thanks are due also to Prof. P. Barry Butler, Dean, College of Engineering and Prof. L.D. Chen, Chair, Department of Mechanical and Industrial Engineering.

I would like to extend heartfelt thanks to my advisor Asst. Prof. Albert Ratner, whose constant guidance, support and encouragement were extremely important for the successful completion of this work. His cheerfulness and lively attitude made this research work a pleasant experience. I wish him and his family a very bright future.

Special thanks are due to the Faculty and Staff of the Chemical Engineering Department for letting me use the laboratory facilities for an important part of this thesis.

Finally, all my labmates – Matt, Majid, Yun, Yan, Xinhui, James, Eric, Taleb, Marta, Brian and Jean, have made my stay in Iowa a memorable experience. I wish these wonderful people best in their lives ahead.

TABLE OF CONTENTS

LIST OF TABLES

LIST OF FIGURES

LIST OF NOMENCLATURE

R_0 (D_0) = Pre-impact radius (diameter) of drop

V_0 (V) = Impact speed (speed)

P_T (P) = Threshold pressure (pressure)

D_L (D_S) = Larger (Smaller) of the two diameters measured for a drop

t = time measured from the instant of impact

t^* = Non-dimensional spreading time

σ_{SV} = Solid-vapor interfacial tension

σ_{LS} = Liquid-solid interfacial tension

σ_{LV} = Liquid-vapor surface tension

d_{max} = Maximum spread diameter

β_{max} = Maximum spread factor

ρ = Density of the liquid

v_L = Kinematic viscosity of liquid

M_G = Weight of one molecule of the gas

γ = Ratio of specific heats of the gas

T = Temperature of the gas

k_B = Boltzmann's constant

ρ_G = Density of the surrounding gas

c_G = Speed of sound in the surrounding gas

δ = Boundary layer thickness

R_A = Amplitude of surface roughness

R_W = Wavelength of surface roughness

r = Radius of the cone of the viscometer

μ_0 = Base viscosity of non-Newtonian liquid

$\dot{\gamma}$ = Strain rate

CHAPTER 1

INTRODUCTION AND PHYSICS

1.1 Background and Motivation

Liquid drop impacts are a very common phenomena occurring in various natural and industrial processes. Applications like fuel injection, spray painting, surface cooling, fire suppression, printing, plasma coating etc. involve a wide variety of drops of various sizes, speeds, and materials, impacting a wide range of surfaces. The outcome of these impacts plays a significant role in determining the effectiveness and efficiency of a particular operation. For example, the ease with which a liquid jet breaks up into fine droplets can determine the quality of fuel injection and hence affect combustion efficiency in an internal combustion engine. In spray cooling of steel slabs, heat transfer can be dependent on how much and how fast the liquid drops spread on the solid surface. Ablation of turbine blades due to drop impacts could be detrimental to engine performance. In addition, drop impact is an example of a complex fluid dynamical problem involving free surface flows with a moving contact line. Such flows are not very well understood, and studying the role of various influencing factors in a drop deformation process could lead to a better understanding of such flows. Owing to these reasons, drop impacts have been studied experimentally, analytically and numerically over a long period of time.

Several factors are of key importance in the deformation of drops upon impact. To better understand the role of these factors, it is important to isolate each parameter of interest and study its effect. The effect of one such factor, the gas surrounding the drop, was demonstrated by Xu et al. [1]. They showed that splashing of a drop on a smooth surface could be suppressed by lowering the pressure of the surrounding gas. They proposed a splashing threshold, whose value was found to be constant beyond a certain critical impact speed. The role of surrounding gas on drop impacts was further

investigated by Dix et al. [2], who studied drop splashing at higher chamber pressures and lower impact speeds, using an experimental arrangement similar to the one used in the present study. One of Dix's conclusions was that at high chamber pressures, the splashing threshold defined by Xu et al., increases with increasing pressure. However, his experimental data was not comprehensive enough to produce clear conclusions. Therefore, to better understand the trends of the splashing limit, the current work focuses on normal impacts of liquid drops of about 2 mm in diameter, on a smooth and dry quartz surface with impact speeds between 1.5-3.5 m/s. The aim was to test several liquids at higher pressures to obtain sufficient splash conditions so that the behavior of the splashing threshold could be properly described. The broader goal of this study is to observe the effect of high chamber pressure on the splash limit and spreading of single drops upon impact.

Another aspect of interest is to assess the effect of pressure on the spreading of drops in the regime below the splash limit. Prior to the current work, Karakaya et al. [3] did initial experiments for drop spreading at high pressures, using pure alcohols as well as a 50:50 mixture of ethanol and methanol. They observed that for pure liquids, maximum spread factor remained constant with pressure while for the ethanol-methanol blend, the spread factor increased, showing an increasing similarity to the spread factor observed for the low viscosity component. The current study looks to further investigate the behavior of spread factor at higher pressures, using better test procedures to overcome the limitations of the previous study. Knowledge generated from these tests could have direct applications in areas like injection and sprays, internal combustion engines, etc. where such high pressure conditions exist. In addition, a well characterized, high accuracy data set will be extremely valuable for validation of computational results of drop impact processes.

The third area investigated was the impact behavior of non-Newtonian liquid drops. Non-Newtonian materials like polymers, gels, slurry, etc. are used in a wide range

of engineering applications. A significant amount of research is being done to characterize impact of such drops on wetting and partially wetting surfaces. In this study, the spreading of drops of diesel-polymer blends have been compared to drops of Newtonian liquid blends at similar impact speeds, with similar base viscosities. Since the deformation of a drop involves strain rates from very high ($\approx 10^5 s^{-1}$) to very low values, it might be possible to capture the effects of shear-dependent viscosities in such drop impacts. Understanding of these aspects could have applications in areas like fuel safety and transportation, where special polymers could be engineered to impart variable viscosity characteristics to the fuel for inhibiting fuel misting in accidents, which in turn could reduce the risk of crash related fires.

Since drop deformation is a relatively fast process, high speed imaging techniques are employed to capture various aspects of the drop impact process. The experimental arrangement used in the present study was built and first used by Dix, Karakaya and co-workers. However, the current study utilizes an improved experimental approach and significantly high camera frame speeds (3500 - 23000 fps) compared to the earlier tests. This provides a more accurate measure of results like spread diameter and average spreading velocities. Well focused images with a resolution up to 0.014 mm/pixel have been obtained for a large number of drops enabling averaging and reduction of experimental uncertainties. The drops selected for analysis were also more uniform in shape compared to previous experiments. Five different liquids including pure alcohols like ethanol, as well as complicated mixtures like diesel, were tested. Unlike Karakaya et al. [3], spread factor tests at high pressures have been carried out at a constant impact speed for ethanol while for other liquids, the change in impact speed due to gas drag has been accounted for. Thus, a more comprehensive set of data has been obtained to better understand the impact behavior of liquid drops under conditions of high chamber pressure, as well as the behavior of polymer-liquid blends.

This introductory chapter further includes a brief discussion on the physics of drop impacts and the effect of different variables on the impact process. That is followed, in chapter 2, by a review of published literature and key findings from prior studies on impacts on dry surfaces. The third chapter describes the experimental configuration and procedures, and is followed by a detailed discussion of the results in chapter 4. Tests with non-Newtonian liquids are discussed in chapter 5 and the thesis concludes with some key conclusions and suggestions for further work in chapter 6.

1.2 Overview of Drop Impacts

Although drop impacts are a common occurrence, the physics behind them is complex and still not well understood. Several variables are involved even in a simple
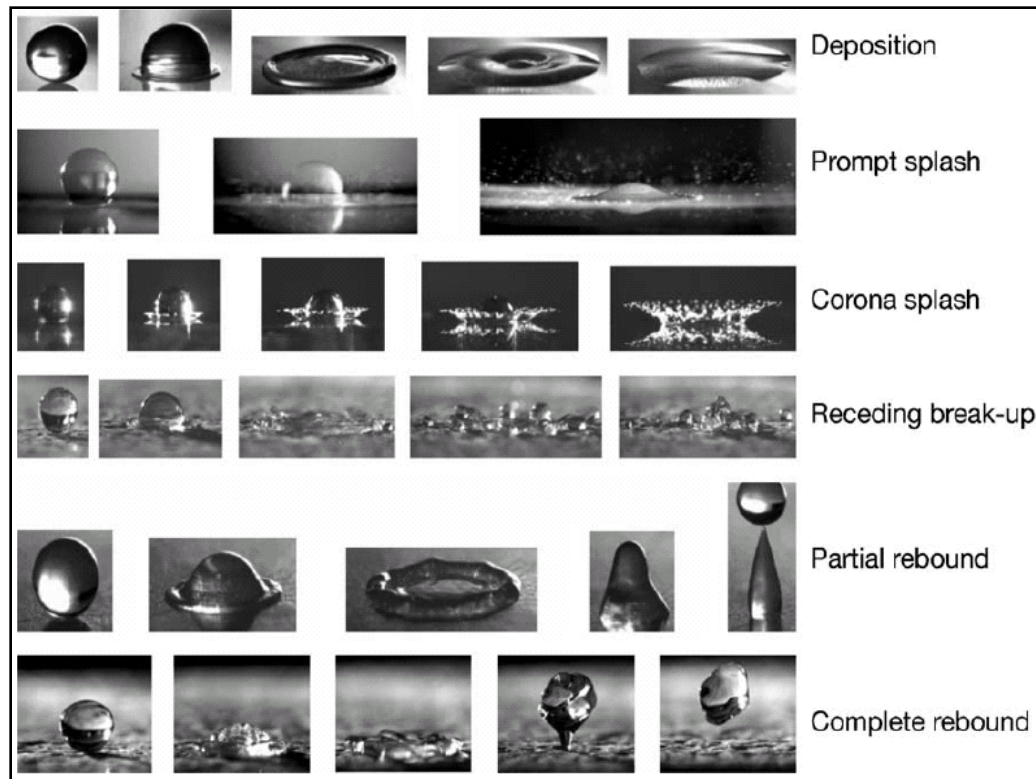
Figure 1.1: Different scenarios in a drop impact on a solid surface [4]

drop impact process, which makes predicting and quantifying its outcome quite challenging. The outcome of drop impact depends on the impact speed, its direction relative to the surface, drop size, properties of the liquid (density, viscosity, viscoelasticity, non-Newtonian effects for rheologically complex fluids), surface or interfacial tension, the roughness and wettability of the solid surface, non-isothermal effects (e.g. solidification, evaporation, etc), air entrapment, surrounding gas pressure, etc. Based on the conditions, a drop can splash, spread, recede or even rebound from a surface as shown in Figure 1.1. Since the present work involves a dry solid surface, the following highlights the general physics behind drop impacts on such a surface.

1.2.1 Physics of Drop Impacts

Spreading of drops on a solid surface is a free surface, moving contact line problem which means that as the drop spreads, new surfaces are formed. The contact line, which is the intersection of three phases – solid, liquid and gas, moves outwards with variable speed. Depending on whether the liquid is fully or partially wetting, the drop can theoretically keep spreading or achieve a static equilibrium shape, respectively. For a non-wetting liquid, the liquid recedes after achieving some maximum diameter. The static equilibrium condition for partially wetting liquids can be described by the Young's equation, as shown by Figure 1.2.

$$\sigma_{LV} \cos \theta_s = \sigma_{SV} - \sigma_{LS}$$

The contact angle is the angle formed between the surface and a tangent drawn to the liquid curvature at the contact line, on the liquid side. For fully wetting fluids, the static contact angle θ_s is very close to 0º; for partially wetting liquids, θ_s lies between 0º - 180º, while non-wetting fluids have contact angles close to 180º.
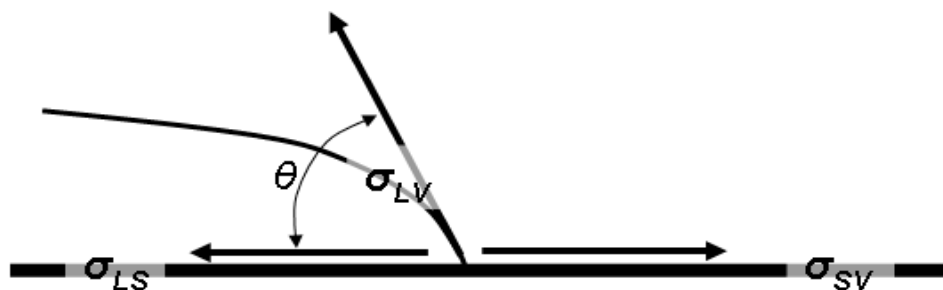
Figure 1.2: Forces acting at the contact line

Impact of a drop on a solid surface can be visualized as interplay of three forces – inertia of the drop or its kinetic energy, surface tension and viscous dissipation. Surface tension and viscosity of the liquid tend to oppose spreading. Prior to impact, if the drop is nearly spherical, the pressure inside is higher than the surroundings and the difference is given by the Young-Laplace equation:

$$\Delta P = \frac{2\sigma}{R_0}$$

As the drop hits the surface, the initial point of contact becomes a stagnation point, due to which high pressure develops there. A displacement wave then travels opposite to the velocity direction, into the drop. This high pressure and change of momentum causes the bottom part of the drop to spread out rapidly as a thin layer called the lamella. This initial phase where the lamella is barely visible, is called the 'kinematic phase' and is governed by inertia and the geometry of the drop. The remaining drop remains unchanged and keeps moving at nearly the impact speed. Due to its thinness, the radial speed of the lamella can be several times higher than the impact speed. As the lamella grows in the 'spreading phase', surface tension and viscosity rapidly decelerate its growth, causing it to thicken near the contact line to form a rim. With drop spreading, the rim grows in thickness as it is fed liquid from the thin lamella. Near maximum spread,

spreading is said to be in a 'relaxation phase' and the contact line speeds approach zero. Once the maximum diameter is attained, waves are reflected inwards from the rim and liquid from the rim travels back towards the center, ultimately resulting in the final static shape. This last phase is called the wetting or equilibrium phase. If the surface tension of the liquid is strong enough, the contact line might recede to a smaller final diameter. For fully wetting liquids, a thin precursor film, usually only several hundred angstroms in thickness, moves ahead of the macroscopic contact line due to intermolecular forces, and the spread diameter keeps increasing with time. Thus, the initial kinetic energy of the drop gets converted into surface energy and viscous dissipation.

Figure 1.3: Early phases of drop spreading. a) Formation of a thin lamella b) Thickening of the lamella to form a rim

Kinematics of the contact line is still debated, and it's not conclusive whether the no-slip condition holds at the contact line or not. In theoretical models, the no-slip condition results in a stress singularity at the contact line. Since contact line movement is driven by molecular wettability, whose speeds are typically lower than the characteristic spreading velocity, severe deformation takes place and the dynamic contact angle approaches 180º. This sort of a motion resembles "rolling" and such a boundary condition helps alleviate singularity at the contact line. Other theories allow for slippage over a small distance near the contact line, include non-Newtonian effects, or propose other modifications to explain the motion near contact line.

An important feature of the contact line movement that affects spreading is the dynamic contact angle θ_d, which refers to the contact angle formed when the contact line is in motion. It differs from θ_s and is found to depend on contact line speed. The dynamic "advancing contact angle" θ_{adv} formed when the spread diameter is increasing, is greater than θ_s, while the "receding contact angle" θ_{rec} is found to be lower than θ_s. This difference in the values of contact angles is called "contact angle hysteresis", and is attributed to chemical inhomogeneities and surface roughness phenomena. Since the contact line is assumed to be of zero thickness, its inertia is negligible and hence a force balance similar to the Young's equation can be written for the dynamic case as:

$$\sigma'_{LV} cos\theta_d = \sigma_{SV} - \sigma'_{LS}$$

where, σ'_{LV} and σ'_{LS} are the liquid-vapor and liquid-solid interfacial tensions, respectively, for the dynamic case, so that they depend on the distribution of the surface parameters along the interfaces, which in their turn are coupled with the bulk flow.

Another common scenario in a drop impact process is splashing, where small droplets are ejected from the main drop upon impact. Two types of splashing are shown in Figure 1.5 – prompt splashing and corona splashing. In prompt splashing, small droplets are ejected from the rim almost instantaneously while the remaining drop continues to spread as usual. Surface roughness is thought to induce this kind of splashing. Conversely, in corona splashing, the spreading lamella lifts off the surface, forming a crown like structure. Fine sub-droplets are then ejected from the corona due to capillary instability. Corona splash is thought to be caused due to the surrounding gas and is enhanced if σ_{LS} is low, which enables lifting.

Splashing is thought to be caused due to the growth of instabilities at the gas-liquid interface. These instabilities can be induced due to surface roughness, the air displaced by the lamella or other factors like drop vibration. Viscosity serves to dampen these instabilities and hence reduce the tendency of splashing. However, if the conditions

are right, the instabilities can grow resulting in finger formation which might then eject droplets due to capillary pinching. Liquids having high viscosity or high surface tension show lesser tendency to splash. At high contact line speeds, since the dynamic contact angle is close to 180º, air entrainment can promote splashing as well as bubble entrapment.

Non-Newtonian drops show certain distinct characteristics in impact behavior. Phenomena like viscoelasticity, variable viscosities, time-dependency of properties, etc. come into play in these impacts. The effective viscosity $\mu_{eff,}$ of commonly occurring rheological fluids is described by the power-law as:

$$\mu_{eff} = \mu_0 \dot{\gamma}^{n-1}$$

If n > 1, the fluid is shear-thickening, i.e., its viscosity increases with strain rate. On the other hand, for n < 1, the liquid is shear-thinning as its viscosity decreases with increasing strain rates.

It is thus clear, that a drop impact process involves interplay of effects from a large number of variables. Some of these aspects are not clearly understood and hence, a complete theoretical or computational treatment becomes extremely complex. Therefore, it becomes vital to study the role of these factors individually and employ simplifying assumptions to reduce the complexity of the problem. One such simplistic method of analysis, based on the conservation of energy in a drop impact process, is explained in the following section. Such an analysis gives a predictive tool to predict post impact results based on pre-impact parameters.
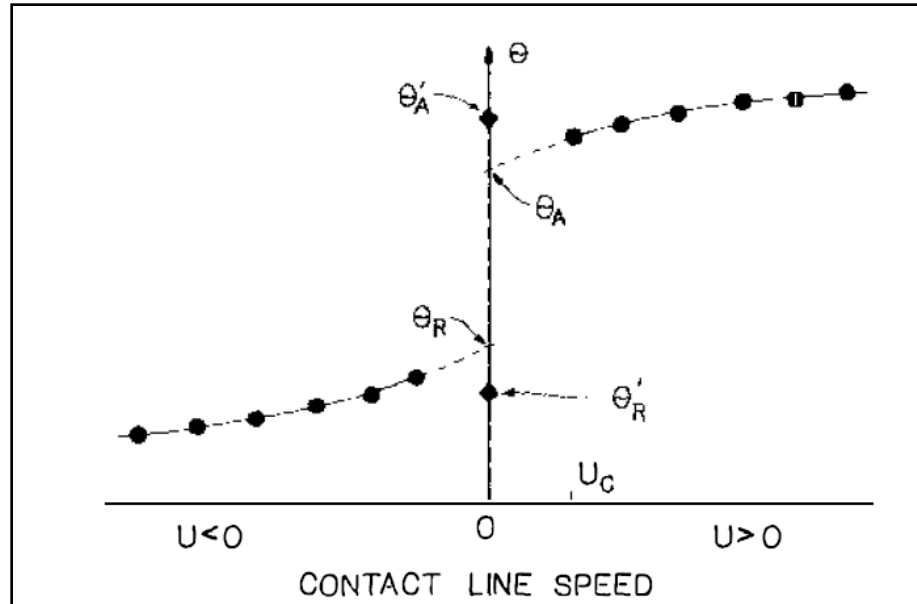
Figure 1.4: Variation of dynamic contact angle with contact line speed.
U>0 represents the advancing phase wile U<0 is the receding phase [5]
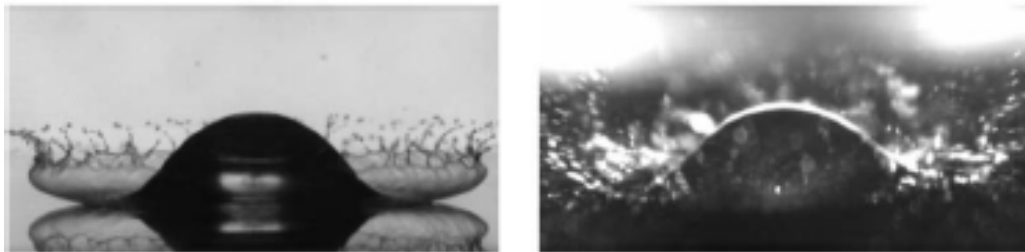
Figure 1.5: Drop splashing scenarios a) Corona splash with ejection from lifted
rim b) Prompt splash on a rough surface. [1]

1.2.2 Energy Conservation Analysis in Drop Impacts

An important parameter of interest in drop impact analysis is the maximum spread factor, which is defined as the ratio of maximum spread diameter of the drop upon spreading, to the pre-impact diameter of the drop, $\beta_{max} = (d_{max}/D_0)$, as shown in Figure 1.6. The relative importance of surface tension, viscosity and inertia in a drop

deformation process is described by certain non-dimensional numbers resulting from dimensional analysis, and are mentioned below:

$$Re = \frac{\rho D V}{\mu} \qquad We = \frac{\rho V^2 D}{\sigma} \qquad Oh = \frac{\mu}{\sqrt{\rho D \sigma}} \qquad Ca = \frac{\mu V}{\sigma}$$

Even though the actual speeds in a drop impact vary with, the above non-dimensional numbers are calculated based on impact speed and diameter. The Reynolds' number (Re) is a ratio of inertia forces to viscous forces while the Weber number denotes a relative comparison between inertia and surface tension of the drop. For high values of these numbers, the impact process is inertia dominated. The Ohnesorge number (Oh) combines all three forces into one parameter. Its value for average drop sizes (~ 3 mm) of common liquids like water and alcohols is around 0.003. The Capillary number (Ca) is normally used to describe the contact line behavior.
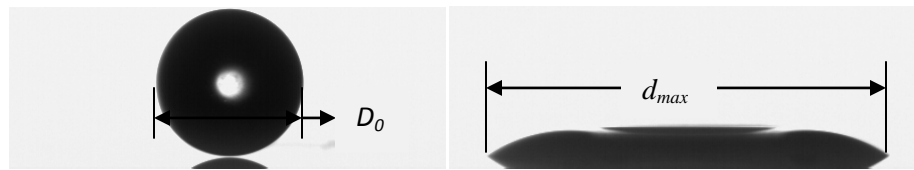
Figure 1.6: Initial and final diameter of a spreading drop

The drop impact process can be looked upon as an energy conversion process. In a drop impact on a solid surface, the pre-impact kinetic energy and surface energy of the drop gets converted to the surface energy of the drop spread and viscous dissipation. Assuming a spherical drop and no splashing, the energy conversion can be summarized as:

$$(E_K + E_{\sigma 1})_{pre-impact} = (E_{\sigma 2} + E_\mu)_{post-impact}$$

The pre-impact kinetic energy is given as:

$$E_K = \frac{1}{2}mV_0^2 = \frac{\pi}{12}\rho V_0^2 D_0^3$$

Surface energies, which depend on the interfacial areas and surface tension, are given as:

$$E_{\sigma 1} = \pi.\sigma D_0^2$$

$$E_{\sigma 2} = \frac{\pi}{4}d_{max}^2\sigma(1 - cos\theta_s)$$

To estimate the viscous dissipation E_μ, an exact analytical expression is very difficult to attain due to the changing shape and velocities. Several simplifying approximations are generally made for velocity gradients and drop shape to enable theoretical development. One such approximation by Chandra and Avedisian [6] gives:

$$E_\mu = \frac{\pi}{4}\mu\left(\frac{V_0}{h}\right)D_0 d_{max}^2$$

Upon substituting these expressions in the original energy balance equation, and non-dimensionalizing it, we get:

$$\frac{3We}{2Re}\beta_{max}^4 + (1 - \cos\theta_s)\beta_{max}^2 - \left(\frac{We}{3} + 4\right) \approx 0$$

Though the above is an approximate analysis, the derived equation can be used to predict β_{max} in terms of the pre-impact parameters and the static contact angle. Several such analytical and experimental models have been developed to quantify a drop impact process, some of which are illustrated in the next chapter.

CHAPTER 2

LITERATURE REVIEW

The first attempt to scientifically study drop impacts was made by Worthington more than a century ago when he studied impact of milk and mercury drops using spark illumination. Since then, the experimental techniques used to study drops have evolved significantly, enabling greater insight into the drop impact process. Concurrently, analytical and computational techniques have increasingly been adopted to describe and predict various impact scenarios. Since drop impacts on dry surfaces are the subject of this work, a review focusing mainly on literature pertaining to such experiments is presented in this chapter. The purpose is to highlight the role of various factors in the impact and deformation process, as investigated in prior published work.

2.1 Overview of Research on Drop Impact on Solid Surfaces

Rein [7] and Yarin [8] compiled comprehensive reviews of drop impact studies which highlight the physics and formulations of impacts on liquid and solid surfaces. For impacts on dry surfaces, Rioboo et al. [4] identified six possible outcomes, as already shown in Figure 1.1. A summary of their conclusions about the effects of several impact parameters on the six outcomes is presented in Table 2.1.

Rioboo et al. [9] and Biance et al. [10] experimentally studied the kinematic phase of an impact ($t^* = t * V_0/D_0 < 0.1$), and found that spreading is independent of liquid or surface properties, and spread diameter varies as $t^{0.5}$ in that regime. Viscosity and surface tension come into effect in the spreading phase, where they oppose inertia to slow down the contact line. Rioboo et al. [9] and Sikalo et al. [11] found liquid viscosity to be more dominant than surface tension in limiting the spread factor. The nature of impact surface and surface tension were found to have an effect only near the maximum diameter, i.e. in

the relaxation phase. For wetting liquids, spreading in the last phase is governed by Tanner's law, $R \sim t^{0.1}$, while partially wetting liquids attain an equilibrium diameter.

Table 2.1: Effect of impact parameters on outcomes of impact on dry surface

Increase of	Deposition	Prompt splash	Receding break-up	Complete rebound	Corona splash	Partial rebound
V	↓	↑	↑		↑	↑
D	↓	↑				
σ		↓	↑	↑	↓	↑
μ	↑	↓	↓		↓	
R_A	↓	↑			↓	
R_W		↓				
θ_{rec}			↑	↑		↑

Source: Rioboo, R., Tropea, C., and Marengo, M., "*Outcomes from a drop impact on solid surfaces",* Atomization and sprays, Vol. 11, pp. 155-165, 2001

Rioboo et al. [8] suggested that this equilibrium diameter lies between a minimum (d_{adv}) and a maximum(d_{rec}) diameter based on respective contact angles, θ_{adv} and θ_{rec}, and are given as:

$$\frac{d_i}{D_0} = 2\left[\frac{sin^3\theta_i}{2(1 - \cos\theta_i)(2 - \cos\theta_i - cos^2\theta_i)}\right]^{1/3}$$

where i represents "advancing" or "receding". Engel [12] studied the evolution of spread diameters, contact line speeds and force exerted on the surface, for impact of water drops on a glass plate using spark schlieren and high speed photography techniques. Both, contact line speed and force exerted, quickly decayed to a fraction of their high initial values. Using energy conservation and a simplified geometry, she derived an expression for the variation of spread diameter with time in the later stages of

spreading, when the drop apex had leveled out. This approach was also adopted in the works of [6, 13-15] to develop expressions for β_{max}, as has been summarized in Table 2.2. All these formulations mainly differ in the modeling of viscous dissipation and assumptions related to drop shape during spreading.

Table 2.2: Proposed models for maximum spread factor β_{max}

Author	Model
Stow & Hadfield [13]	$\beta_{max} = C\sqrt{\left(2(We + 2We/Fr + 6)\right)/\left(3(1 - \cos\theta_s)\right)}$
Chandra & Avedisian [6]	$(3We\beta_{max}^4/2Re) + \left(\beta_{max}^2(1 - \cos\theta_s)\right) - (We/3) - 4 \approx 0$
Scheller & Bousfield [15]	$\beta_{max} = 0.61(Re^2 Oh)^{0.166}$
Scheller & Bousfield (Free Spreading)	$\beta_{max} = 0.91(Re^2 Oh)^{0.133}$
Pasandideh-Fard et al. [14]	$\beta_{max} = \sqrt{(We + 12)/\left(3(1 - \cos\theta_s) + 4\left(We/\sqrt{Re}\right)\right)}$
Fukai et al. [21]	$(We/2Re^{0.772})\beta_{max}^4 + \left(2.29(1 - \cos\theta_s)\right)\beta_{max}^3 - ((We + 12)/3) = 0$
Ukiwe & Kwok	$\left((3(1 - \cos\theta_s)\sqrt{Re} + 4We)/\sqrt{Re}\right)\beta_{max}^3 - (We + 12)\beta_{max} + 8 = 0$

Stow and Hadfield [13] neglected viscous dissipation in their analysis, resulting in an inaccurate expression for β_{max}. Chandra and Avedisian [6] assumed the final shape of the spread as a flattened disk of thickness *h* and diameter d_{max}. Taking *h* as the length scale for viscous forces, they derived a fourth order equation in β_{max} for an isothermal impact. Pasandideh-Fard et al. [14] improved this analysis by using a non-dimensional boundary layer thickness $\left(\delta = 2\,D_0/\sqrt{Re}\right)$ as the characteristic length scale. Scheller and

Bousfield [15] modeled the spreading drop as a cylindrical liquid column being squeezed between two parallel plates. Because of such simplifications, these models can only roughly predict β_{max} for general impact situations.

Chandra and Avedisian [5] studied non-isothermal effects for impacts of n-heptane drops on a heated metallic surface, from room temperature up to the Leidenfrost temperature. They observed that with increasing surface temperature, contact angles increased, resulting in lower spread diameters. Evaporation and boiling become increasingly important causing pattern formation and an increased tendency of recoil. Bubble entrapment was noticed near the impact point which was attributed to cavitation resulting from high radial flow speeds. Such bubble entrapment was also noticed in the experiments of Fujimoto et al. [8]

Elliott and Riddiford [16] measured the dynamic contact angles for a liquid film moving between two parallel plates and observed that θ_{adv} attains a maximum value for a given liquid-solid combination, beyond which it is independent of speed. Pasandideh-Fard et al. [13] studied the effect surfactant concentration on water drop impacts, and found that the maximum value of θ_s was close to 110º for all concentrations, while θ_s decreased with increasing surfactant concentration. At high enough Weber numbers, maximum spread factor was found to depend only on Reynolds number. Several analytical expressions for θ_d are available in literature. As listed in the review by Yarin [8], the correlation by Jiang et al. predicts θ_d in terms of θ_s and Ca, and is given as:

$$\frac{\cos\theta_s - \cos\theta_d}{1 + \cos\theta_s} = \tanh(4.96\, Ca^{0.702})$$

More investigations on contact line behavior and wetting characteristics can be found in the works of Dussan [5], Sikalo et al. [17], Cox [18] and Basaran et al. [19]. The effect of viscosity on drop impacts has also been studied extensively in [1, 15]. Scheller and Bousfield [15] used mixtures of glycerol and water with viscosities up to 300 mPa-s.

Spread factors were found to decrease with increasing viscosity, and towards very high viscosity values, spread factors were almost independent of impact speed.

Besides the experimental studies, drop spreading below the splash regime has also been analyzed numerically and analytically by several authors. Harlow and Shannon [20] were the first to solve the Navier-Stokes equations for an incompressible, viscous drop using a Marker-and-cell technique. Fukai et al. [21] simulated a drop impact using finite element method. He dispensed with the no-slip condition at the contact line by assuming that the liquid slips tangentially to the solid surface. Though the final spread factors were grossly over-predicted, the results for the initial stages of impact were in good agreement with experimental observations. Concepts like slip over a small length, presence of non-Newtonian effects at contact line, etc. have been proposed as a solution to the stress singularity at the contact line.

Pasandideh-fard et al. [13] applied the 3D VOF method for simulation. They applied the measured values of θ_d to their numerical model which yielded better spread factor results compared to the cases using constant θ_s. Bussman et al. [22] simulated 3-D drop impacts with significant receding while Reznik and Yarin studied impacts on inclined surfaces through numerical methods. Cox [18] used the method of matched asymptotics to analyze flow at the contact line by dividing the drop into three regions. Roisman et al. [23] used the mass and momentum balance equations for the free rim, with allowance for the inertial, viscous and surface tension forces and capillary effects, and were successfully able to predict the growth and shrinkage of the spreading drop.

Splashing of drops on a solid surface has been another aspect that has received considerable attention in literature. As inertia of the drop increases, impact results in creation of instabilities at the rim of the spreading lamella. Introduction and growth of such instabilities is assisted by surface roughness, liquid properties, surrounding gas, etc. The main focus in literature has been to quantify the criteria for splashing, mainly in

terms of critical values of parameters like the Weber Number, and to study and simulate the mechanism of instability growth resulting in drop break-up.

Splashing on solid surfaces was first described qualitatively by Engel [12] and Levin and Hobbs [24], who observed that increase of drop inertia resulted in drop splashing and that, surface roughness could trigger splashing. Stow and Hadfield [13] described this role of surface roughness in terms of a splashing constant S_T, given as a product of certain indices of impact Reynolds and Weber numbers. The critical value of S_T depended only on surface roughness, and splashing was observed when S_T for an impact exceeded the critical value. A summary of various splashing criteria is mentioned in Table 2.3.

Table 2.3: Proposed criteria for transition from spreading to splashing.

Author	Model
Stow & Hadfield [9]	$Re^{0.31}We^{0.69} = (2\rho/(\mu^{0.31}\sigma^{0.69}))f(R_a)$
Mundo et al. [15]	$Oh \times Re^{5/4} > K, \ \ K = f(R_a)$
Cossali et al. [26]	$Oh \times Re^{5/4} > 119.23$
Range and Feuillebois [25]	$We > We_{crit}(\approx 310)$, for $Oh \leq 0.02$
Vander Wal et al. [16]	$Oh \times Re^{0.609} > 0.85 \ \ \ \Rightarrow Ca_{crit} = 0.1225$ approx.
Xu et al. [1]	$\sum_G/\sum_L > 0.45$, (See section 2.1 for details)

A general consensus is found in literature on the role of surface tension in splashing of liquid drops on dry surfaces. A liquid with high surface tension shows lesser

tendency to splash as the surface tension tries to keep the drop together. However, once the instabilities set in, finger formation and final pinch off is driven by capillarity. Viscosity serves to dampen the instabilities and hence opposes splashing. But, interestingly, within a certain range of values, viscosity seems to promote splashing as mentioned in [1, 2, 15].

Mundo and Sommerfield [25] derived a splash criterion in terms of Reynolds and Ohnesorge numbers, by impacting a stream of small drops (60-150 µm) on a rotating stainless steel disc with two roughness values. The impacts were effectively oblique to the surface. They formulated a splashing criterion in terms of Reynolds and Ohnesorge numbers based on only the normal component of impact speed. Cossali et al. [26] came up with a similar expression as Mundo; however, he specified the value of the critical constant ($K = 119.23$) above which splashing took place.

Range and Feuillebois [27] used mixtures of water and ethanol to vary the liquid surface tension. They observed that the critical Weber number for splashing depends also on the combination of liquid and surface material, due to the variation of contact angles. Vander Waal et al. [28] studied the impact of twelve different liquids on a highly smooth metallic surface under atmospheric condition. With certain simplifications, they expressed the splash criterion in terms of a critical Capillary number.

More recently, Xu et al. [1, 29] showed that splashing on smooth surfaces is affected by the nature and pressure of the surrounding gas in which impact takes place. Their results are discussed in detail at the end of this chapter. They also studied impacts on rough surfaces and concluded that corona splash takes place on smooth surfaces and is affected by the surrounding gas, while prompt splash is promoted by surface roughness. Jespen et al. [30] studied the impacts of large drops (~ 10 cm), both experimentally and numerically. They noticed that, just prior to impact, the speed of air between the drop and the surface can be as high as ten times the impact speed. They concluded that air

entrainment causes Kelvin-Helmholtz type instabilities, which may grow and result in splashing.

Rein and Deplanque [31] reviewed all the above splash criteria and formulated them in terms of critical Ohnesorge and Reynolds numbers $\left(Oh_{crit} = \alpha Re^{\beta}\right)$. They suggested that, for smooth surfaces, air entrainment at the rim of the expanding lamella induces onset of splashing. An order of magnitude comparison between the critical Capillary numbers for air entrainment $\left(Ca_{crit,AE}\right)$ and splashing $\left(Ca_{crit,splash}\right)$, showed that the former is generally smaller. This implies that air entrainment doesn't always result in splashing. They attributed this non-occurrence of splashing even when air entrainment occurred, to phenomena like "hydrodynamic assist" and small gap effects between the surface and the lifting lamella.

Considerable work has been reported on the mechanism of growth of azimuthal perturbations, number of fingers formed and break-up of corona. Both Rayleigh-Taylor and Kelvin-Helmholtz mechanisms have been cited for instabilities behind fingering in the drop. The initial perturbations grow due rapid deceleration of the lamella. According to Allen [32], the fastest growing wavelength, $\lambda = 2\pi[3\sigma/\rho a]^{0.5}$ (a is the deceleration), dictates the number of fingers, given as $N_f = 2\pi R_{max}/\lambda$. Like Rein et al. [31], Thoroddsen and Sakakibara [33] suggested air entrainment as the likely cause of finger formation. They showed that the final value of N_f cannot be traced directly back to the initial number of fingers because of their splitting and merging, which is not accounted for in the RT-instability theory. Besides, the works of Xu et al. [29] and Jepsen et al. [30] have suggested Kelvin-Helmholtz instability as the likely mechanism of splash inception.

Surface roughness dramatically changes the fingering and splashing pattern. Range and Feuillebois [27] showed that as roughness is increased, the number of fingers decreases. Xu et al. [29] reasoned that splashing occurs due to disturbances induced in the lamella when its thickness is of the order of roughness amplitude. If the lamella thickness is much smaller or larger than the roughness features, no splashing is observed

Several other articles have explored the role of different influencing parameters on the dynamics of drop impacts through numerical and analytical methods. This review has thus highlighted some key aspects related to impacts on solid surfaces. Surface tension, viscosity, contact angles and nature of impact surface, surface roughness and surrounding gas have been shown to have important effects on the outcome of such impacts. However, one thing that emerges is that there are still several things not clearly understood about this phenomenon. Liquid movement and its interaction with the solid surface near the contact line is not fully clear due to limitations of both experiments and theories. The singularity at the contact line resulting from no-slip condition at the solid surface appears to be the most challenging aspect in numerical simulations of drop impacts, even though numerical studies have broadly been able to predict other aspects of the outcome of a drop impact process. As a whole, there seems to be no single theory or criterion that can predict spreading or splashing for all conditions. The current work is another step towards having a better predictive ability about the outcome of drop impacts on a smooth surface.

2.2 Role of Surrounding Gas on Splashing on Smooth Surfaces: Xu et al. [1]

Xu et al. [1] demonstrated that nature of the surrounding gas affects splashing of a drop on a smooth surface and that, splashing could be suppressed by sufficiently lowering the pressure of the surrounding gas. As shown in Figure 2.1(b), it was found that the threshold pressure P_T, at which splashing is first observed decreases with increasing impact speed for a given drop. This means lower pressures are required to suppress splashing at higher speeds. Considering the stresses due surrounding gas and that due to surface tension in the liquid at the contact line, they defined a splashing ratio as:

$$\frac{\Sigma_G}{\Sigma_L} = \frac{P_T}{\sigma} \sqrt{\gamma M_G} \sqrt{\frac{R_0 V_0}{2 k_B T}} \sqrt{\nu_L} \tag{1}$$

Here, $\sum_G$ refers to the restraining stress exerted by the gas due to its compressibility. Since the lamella accelerates extremely rapidly in the earliest stages of its formation, an effect similar to water hammer is assumed to occur in the gas for which the stress is given as $\sum_G \sim \rho_G c_G V_0$. The internal stress due to surface tension is approximated as $\sum_L = \sigma/\delta$. This expression is clearly an approximation since surface tension acts only at the interface, and it seems that the approximation is valid only because the lamella is very thin. Xu et al. stated that splashing occurs when these two stresses are comparable. This splashing ratio was found to have a constant value of 0.45 for impacts at speeds higher than a certain critical speed V^*, that varied with the liquid used. It was stated that a drop having a splashing ratio greater than 0.45 in this regime would splash, while no splashing would occur for a value lower than 0.45. The expression suggests that the likelihood of splashing increases with increasing molecular weight of the surrounding gas, drop size and impact speed, and kinematic viscosity of the liquid.

The above study however, did not characterize the behavior of the splashing limit at speeds lower than the critical speed. As was introduced earlier, it is one of the goals of this work to investigate the role of surrounding gas in splashing of drops at low speeds, particularly by inducing splashing at elevated pressures. Drop impacts under high pressure conditions are observed in applications like fuel injection in internal combustion engines. Hence, this study is not only theoretically useful in understanding drop deformation physics but can also provide useful insights for better design of practical systems.
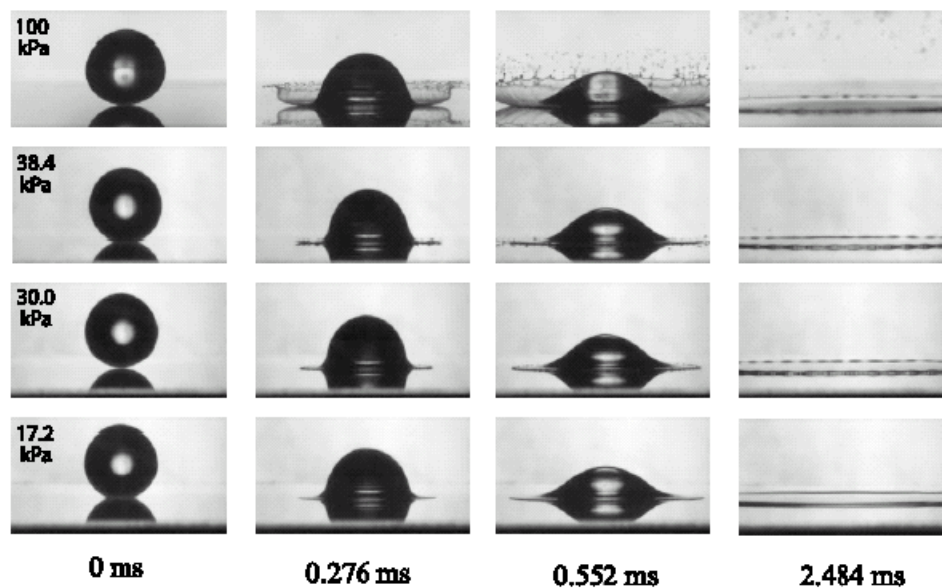
(a)
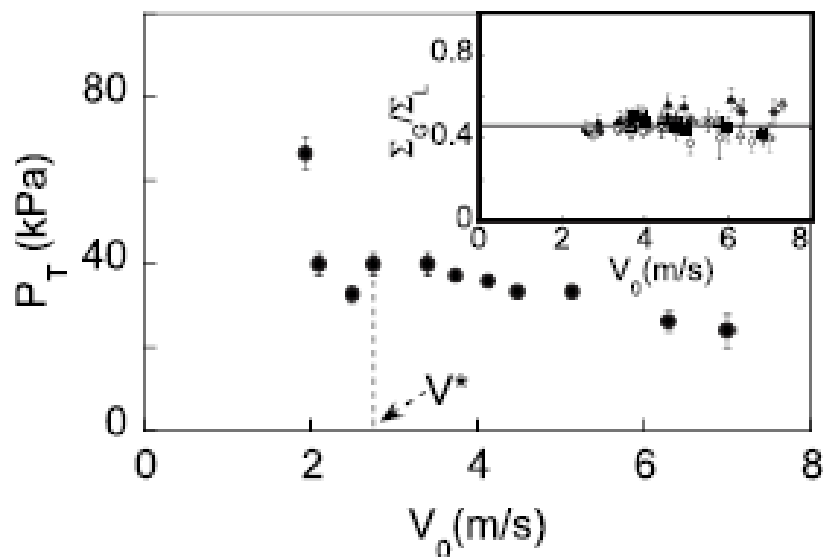
(b)

Figure 2.1: Effect of surrounding gas on splashing a) Suppression of drop splashing on a smooth surface; $P_T = 38.4$ kPa b) Variation of threshold pressure and splashing ratio (inset) with impact speed [1]

CHAPTER 3

EXPERIMENTAL ARRANGEMENT AND PROCEDURE

For meaningful experimental studies, it is of utmost importance to generate an accurate and repeatable set of data using a good experimental set-up and careful testing procedures for minimizing errors. The experimental arrangement used in the present study primarily consists of a pressure chamber with a fixed impact surface, a drop generator, and a high speed camera for capturing the images. The pressure chamber is rated for operation at pressures up to 20 bars. Such a system offers great visibility and impacting drop repeatability. Testing procedures used were somewhat different for splashing, spreading and polymer-blend tests. A portion of the experiments related to viscosity measurements of test liquid mixtures was conducted at the Unit Transport Laboratory using a Brookfield Cup and Cone type digital viscometer, and is described in chapter 5. The following sections of this chapter describe in detail the main experimental configuration, procedure of data collection, experimental parameters and the analysis techniques employed.

<u>3.1 Experimental Configuration</u>

A schematic of the experimental arrangement is shown in Fig 2.1. The arrangement mainly consisted of a pressure chamber with a 6"x6"x6" working volume for testing. It was constructed by welding together four steel C-sections forming the side-walls which were then welded onto a thick steel base. A flange was welded on the top portion of the walls to enable bolting of a lid for sealing the chamber. The C-sections had 6"x6" cutouts in them where four 44 mm thick transparent windows were affixed for viewing the impacting drop. Two of these windows, which are in line with the high speed camera, are made of polished quartz for undistorted imaging, while the other two were polycarbonate windows to enable viewing by the experimenter. Inside the chamber, a 5"

diameter cylindrical quartz block was fixed as the impact surface. The block was made of highly refined NSG "N" quartz material, smoothed to $1/4\lambda$ ($\lambda = 619$ nm) across a 5.08 cm
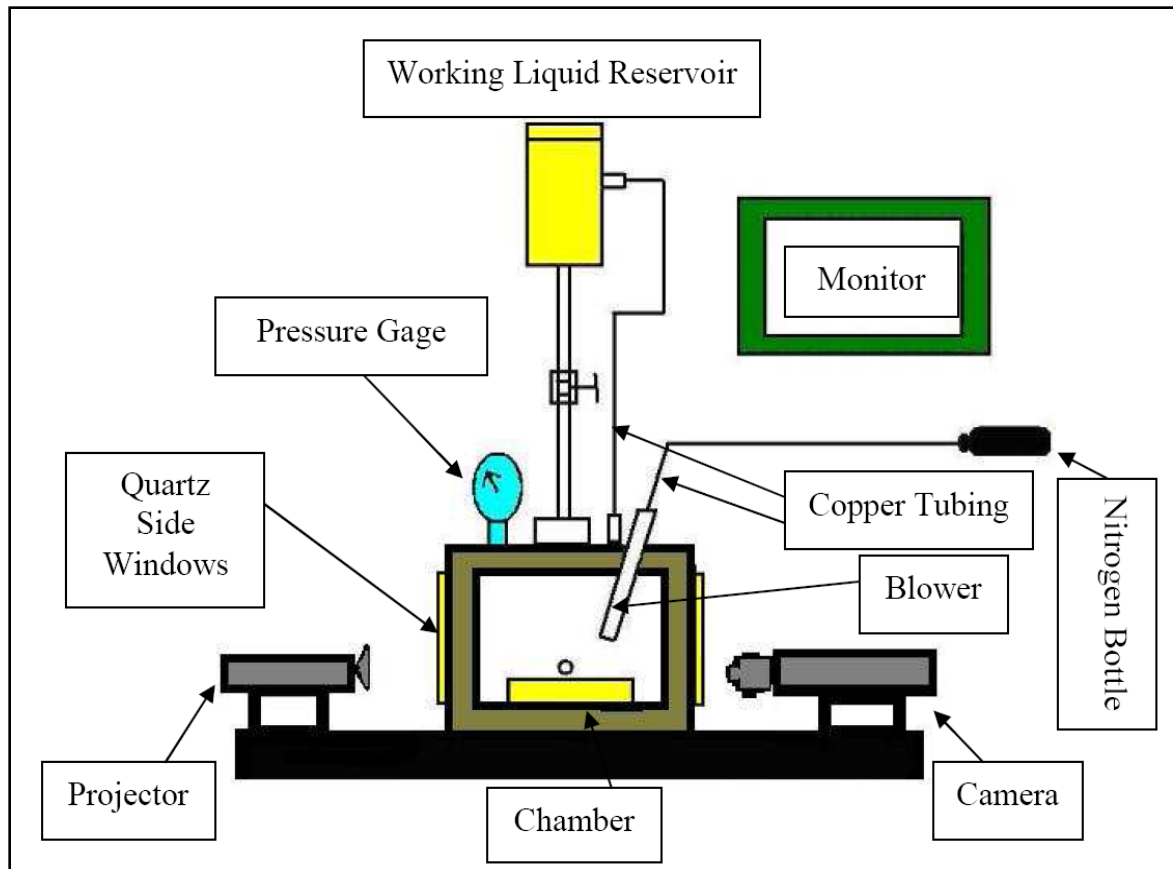
Figure 3.1: Schematic representation of the experimental arrangement

diameter area. Such high degree of flatness and surface finish ensured that only the effects of pressure on drop impacts could be isolated, while effect of surface roughness, inclination, etc. was eliminated. Since the tests were to be carried out at high pressures, pressurized nitrogen stored in external gas cylinders could be supplied to the chamber through a pipe running through one of the four ports on the top lid. Nitrogen was used as the medium since it provides an inert atmosphere and is readily available. A pressure

gauge mounted on the top lid could measure chamber pressure to an accuracy of 1 psi. Further details of design and construction of the pressure chamber can be found in [2, 3].

A blunt-end hypodermic needle, enclosed in transparent PVC tubing and mounted on the top lid of the pressure chamber, was used as the drop generator. This tube-needle assembly was fastened using end connectors from Swagelok, to an adaptor mounted on the top lid. Two different needle sizes, 23 gauge and 17 gauge, were used to generate drops of roughly 2.1 mm and 2.7 mm in diameter, respectively. The height of the needle could be increased by assembling additional pipe elements which allowed the variation of impact speed. Test liquid was supplied to the needle from an overhead reservoir through a PVC pipe with a ball valve and a needle valve in between to regulate flow through the needle. The liquid reservoir was connected to the main pressure chamber using a ¼" copper tube so that the two were at equal gas pressure. This ensured that there was very minimal pressure difference across the needle, and that the drops detached from the needle only under the effect of gravity. Any pressure imbalance was undesirable as it could either force bubbles into the liquid in the tubing, or cause forced ejection of drops from the needle. All tubing connections were made using steel fasteners from Swagelok.

The impacting drops were videographed approximately normal to the direction of incidence using an IDT XStream-Vision XS-3 digital camera with a Nikon 105mm f/2.8D Micro-Nikkor lens. A 300 W projector lamp was used to create a bright background against which sharp images of the falling drops could be visible. A millimeter scale was used to obtain the calibration factors for conversion from pixels to millimeters. Details of the experimental procedure, as given below, further highlight the parameters employed in the current experiments.

3.2 Experimental Procedure

The three types of tests mentioned earlier – splashing, spreading and tests with diesel-polymer blends were carried out with the arrangement described above. However,

the methodologies adopted were quite different in these tests due to the different objectives. This section highlights the procedures applied for the individual tests.
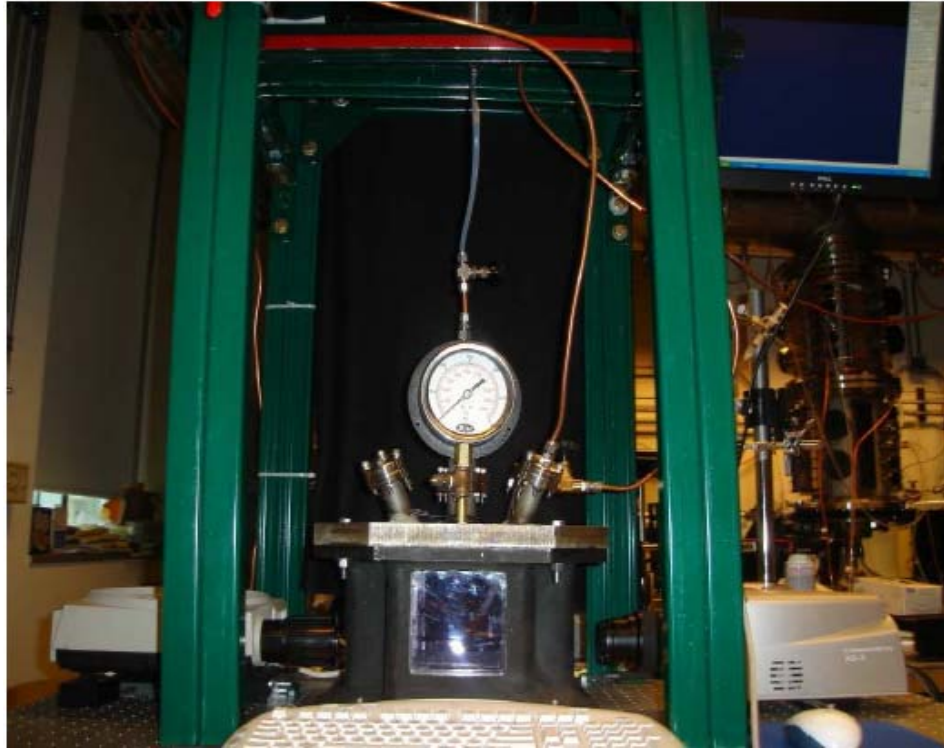
Figure 3.2: Photograph of the experimental arrangement

3.2.1 Splashing Tests

To study the effect of chamber pressure on splashing and spreading of pure liquid drops, tests were carried out at pressures up to 12 bars. The main variables in the tests were chamber pressure, impact speed, type of liquid and drop size. The liquids ranged from common alcohols like ethanol, to a complex mixture like diesel. Drops nearly 2.1 mm and 2.7 mm in diameter were used for the study. Impact speed could be varied by changing the height of the needle using additional pipe attachments. However, the height could be increased only in 2" increments. Since the experimental procedure was nearly

identical for the two types of tests, a brief, step-by-step summary of the experimental procedure is given, and then further details and differences are mentioned subsequently.

1. Setting the needle valve and needle height

   The overhead reservoir was filled with test liquid and the liquid was allowed to run through the needle to eliminate any trapped bubbles in the liquid line. The needle valve was set to a fixed small opening for slow drop formation with opening or closing of the ball valve.

2. Setting and focusing the camera

   The camera was set to capture images at about 3000-4000 fps with sufficient background brightness and field of view, so that the full drop was visible in at least one of the frames. The lid of the chamber was bolted in place and the needle was mounted on top of it. The pressure release valve was closed and the chamber was pressurized to the desired level. Several trial drops were then allowed to fall and recorded by suitably adjusting the camera focus. Once the images were obtained to desired sharpness and clarity, the pressure was released and the lid unbolted.

3. Cleaning the impact surface

   The impact surface was cleaned using xylene and acetone while it was wiped dry using lintless lens cleaning tissues. Once the cleanliness of the surface was ensured, the lid was closed again.

4. Imaging and recording drops

   For collecting actual data, the camera was set to record around 3000 frames giving a total recording time of nearly 1 second. The chamber pressure was set to the desired level and then a single drop was allowed to fall off the needle slowly under the effect of gravity. Just before the drop got released, the camera was manually triggered to capture the entire impact process. Fifty to sixty frames spanning the period of interest, depending on the test objective, were saved.

5. Repeat steps 3 and 4

   Steps 3 and 4 were repeated to obtain 10 to 15 drops at the given pressure condition to average out the minor variations. Only in-focus and nearly spherical drops were saved.

6. Calibration and calibration factor

   Once all drops were recorded for a given test pressure, the lid was taken off and a standard millimeter scale was photographed to desired sharpness in the same focal plane as the drops without changing the focus setting. Two different images were obtained to calculate an average calibration factor.

Drop sizes from the two needles were found to be dependent on factors like the properties of the liquid used, needle valve opening, chamber pressure, etc. It was noted that drop size increased slightly with higher flow rate through the needle. The reason for such an increase has been explained in literature and might be due to dynamic effects of pinch-off. Also, towards higher chamber pressures, the drop size was seen to increase and the drop shape got increasingly distorted. Therefore, a careful adjustment of the valve opening was required to minimize such distortions. A variation of 5% was noticed in the equivalent drop size across the entire range of tested pressure. However, drop distortion, measured as the difference in the largest and the smallest diameters of a drop, was as high as 12%. Drops beyond this limit were rejected for being out of shape.

Splash tests were carried out using ethanol and methanol for impact speeds between 1.7 – 3.3 m/s. The main idea was to determine the threshold pressure at a particular impact speed of a given drop size. This was done by having drop release from a certain height at different chamber pressures until the drops were found to splash, with a few small droplets breaking away at low angles to the impact surface. Several such threshold pressures were obtained for different needle heights for the two liquids. Using the captured images, splash threshold was calculated as described in the analysis section.

3.2.2 Spreading Tests

Spread tests were carried out using four different liquids – ethanol, n-propanol, n-hexadecane (cetane) and diesel. As mentioned previously, unlike Karakaya et al. [3] who obtained drop impacts from a constant height, two different testing techniques were used in the present study. It was realized that for a constant height of drop release, the impact speed reduces with increasing chamber pressure due to the increased gas drag on the drop. One such variation of impact speed is shown in Fig 3.3. The maximum spread factor in turn, depends strongly on impact speed for a given drop size. Hence, comparison of spread factors at different chamber pressures with drops released from the same height would not give the appropriate comparison. Therefore, ethanol drops were tested up to a chamber pressure of 7.2 bars at a nearly constant speed of 1.75 m/s. The change in the impact speed due to gas drag was compensated for by increasing the needle height, and then suitably adjusting the chamber pressure to a higher value, so that the impact speed was maintained as nearly constant as possible. This technique helped to better isolate the effect of chamber pressure on spread factor.

For propanol, cetane, and diesel however, the same technique could not be adopted due to limitations of the experimental arrangement and tendency of these drops to splash easily. With the arrangement used, the minimum impact speeds achievable at atmospheric pressure were around 1.7-1.8 m/s. Close to these impact speeds, the three liquids showed splashing especially as the chamber pressure was increased. Hence, these liquids were tested from the minimum height possible such that, as the pressure was increased, impact speeds reduced sufficiently, avoiding any splashing. Chamber pressures up to 12 bars were used beyond which drop distortion was considered unacceptable. Impact speeds were in the range of 1.5 – 1.7 m/s. Drop impacts were then obtained at atmospheric pressure with the chamber open, at speeds corresponding to each of the high pressures used. The effect of pressure on maximum spread factor could then be studied by comparing the spread factors at atmospheric pressure and higher pressures. Unlike the

tests with ethanol, drop impacts were obtained on replaceable 1 mm thick transparent glass slides because it was difficult to clean the residual drops.

The data images collected were analyzed manually as per the process detailed below to obtain the relevant results. Results of these tests are discussed in the following chapter.
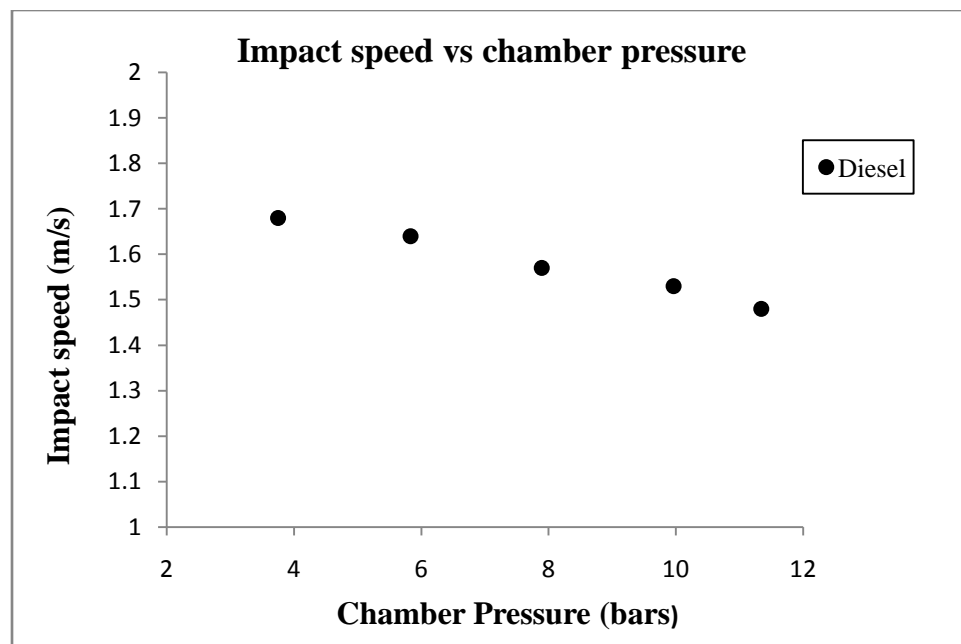

Figure 3.3: Variation of impact speed with chamber pressure for drop release from a constant height

3.3 Analysis

Images of drops obtained were analyzed manually to calculate values of drop diameter, impact speed, maximum spread factor, contact line speeds, etc. For each set of drops, the first step was to obtain a calibration factor to convert pixel readings into millimeters. Distance (in mm) between two extreme graduations visible in the image of the scale was divided by the pixels separating them, as read off the screen, to obtain a calibration factor in mm/pixel. An average calibration factor was obtained by averaging

the values obtained from the two images of the scale. Drop diameters were read off the screen by measuring pixel distance between two diametrically opposite points. Since the drops deformed due to gas drag and were not perfectly spherical, diameters were measured along both the horizontal and the vertical axes. Assuming symmetry in the azimuthal direction, the drop was considered as an ellipsoid for which an equivalent diameter D_{eq} was calculated as $D_{eq} = (D_L^2 D_s)^{1/3}$. This diameter, in pixels, was converted to millimeters by multiplying with the average calibration factor. The distortion of the drop was measured as a percentage of the equivalent drop diameter and was given as:

$$distortion \% = \frac{D_L - D_S}{D_{eq}} \times 100$$

This distortion was as measured in the last two frames prior to impact. Since the field of view of the camera focused very close to the surface, it was not clear whether the drops oscillated during the fall or not.

Impact speed was obtained by dividing the distance travelled by a drop in the last two frames prior to impact, by the time interval between the two frames. The impact speed, along with the equivalent diameter, was used to calculate parameters like the non-dimensional numbers and the splash ratio. Spread factors for a deforming drop could be calculated at each time interval by dividing the spread diameter at that instant by D_{eq}. As shown in Figure 3.4, spread diameters were calculated using the diameter of the lamella d_{lam}, instead of the contact line diameter d_{cont}. This is because the location of the contact line could be precisely determined due to the limitations of the photography technique. Spreading velocities for a given drop impact were calculated at each time instant by dividing half the change of spread diameter between two successive frames, with the time interval between the two frames, i.e.,

$$V_k = \frac{(d_{k+1} - d_k)}{2 * \Delta t}$$

where, k denotes the current frame, V_k denotes the spreading velocity at the time instant corresponding to frame k, d_k is the spread diameter in the current frame, d_{k+1} is the spread diameter in the next frame and Δt is the time interval between successive frames depending on the frame speed used. As seen from Figure 3.4, since the difference between d_{lam} and d_{cont} is relatively small and does not change appreciably over time, the contact line speeds could be assumed equal to the spreading velocities V_k.
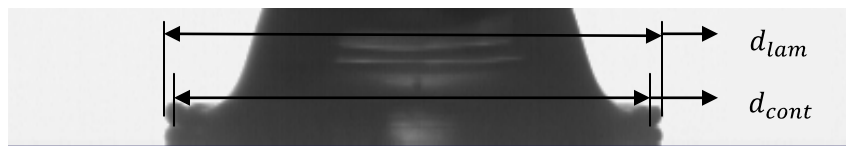

Figure 3.4: Diameter of the spreading lamella and diameter of the contact line

Since, there were variations in the values of the quantities measured, an average value of parameters like drop diameter, impact speed and maximum spread factors was calculated by taking the arithmetic mean of all values of that parameter under a particular condition. Error bars were then created using standard deviation of the data set to judge the preciseness of the tests. All data have been reported at a 95% confidence level.

$$\bar{x}_i = \frac{1}{N}\sum_{i=1}^{N} x_i$$

It should be mentioned that, for the splashing threshold tests, threshold pressure for a particular speed was taken to be the average of the pressures at which ejection of a few secondary droplets from some drops were first seen, and that at which secondary droplets broke away from the drop at low angles to the surface in all directions. MS-Excel was used to tabulate, calculate and plot the different sets of results which are presented in the following chapter.

Table 3.1: Physical properties of liquids

Liquid	Density at 20 °C (kg/m^3)	Viscosity at 20 °C (mPa-s)	Surface tension at 20 °C (mN/m)
Methanol	791.8	0.59	22.70
Ethanol	789.0	1.20	22.10
n-propanol	803.4	1.97 (25℃)	23.70 (25℃)
n-hexadecane	773	3.507	28.12
Diesel	~830	3.61 (25 °C)	~28.0
Iso-butanol	805	3.77 (25 °C)	24.0
Glycerol	~1200	~1500	63.0

Source: Journal of Chemical Data, 1998 43(3)

CHAPTER 4
EXPERIMENTAL RESULTS AND DISCUSSION

Drop impacts were obtained on a dry and smooth quartz surface at different chamber pressures, as per the procedure described in chapter 3. Impact speed, chamber pressure, drop size and the type of liquid were the key variables of the experiments. To be sure that the experiments were working well, initial tests were performed at atmospheric pressure at different impact speeds so that comparisons could be made with previous tests and models. β_{max} was found to increase with impact Reynolds' numbers which is an expected and known result, since higher Reynolds number means either high inertia (speed or size) or low viscosity. As shown for methanol in Figure 4.1, β_{max} was found to increase linearly with Reynolds number.
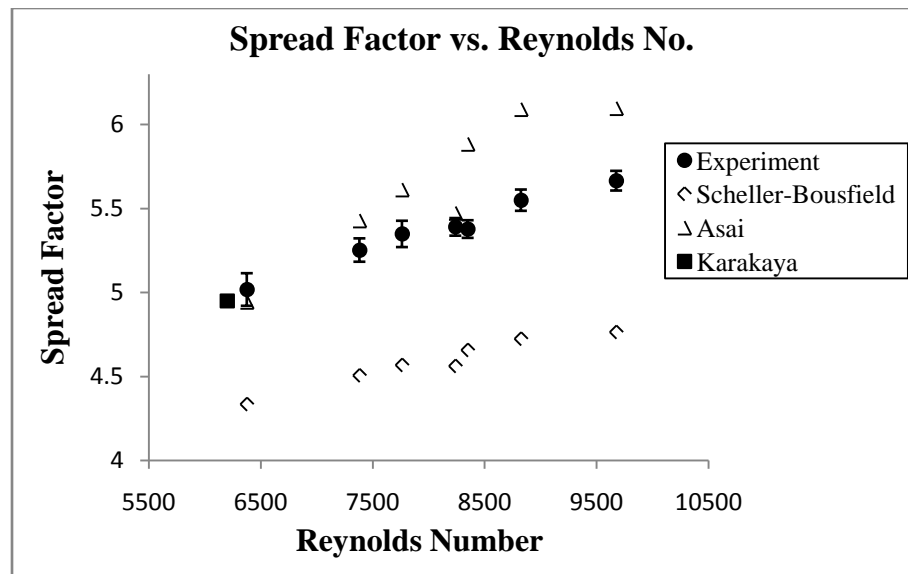

Figure 4.1: Comparison of experimental β_{max} with known results and models at 1 bar.

Figure 4.1 also shows a comparison of β_{max} values from the current experiment with the values obtained by Karakaya et al. [3] and also those predicted by empirical

models of Scheller & Bousfield [15] and Asai et al. [34]. These two models were specifically chosen for comparison since they predict β_{max} in terms of impact non-dimensional numbers only, unlike other models which involve measurement of θ_s. The experimental results of Karakaya et al. were obtained at comparatively lower impact speeds and hence only one instance from his experiments is shown. It can be seen that the current results are in good agreement with the results obtained by Karakaya et al. The model proposed by Asai shows a good match with the experimental results at lower Reynolds' numbers; however it tends to over-predict β_{max} at higher Reynolds' numbers. On the other hand, the "free spreading" model given by Scheller and Bousfield under-predicts β_{max} by about 15%; however, β_{max} predicted by their model follows the increasing trend of the experimental results better than those predicted by Asai's model. This difference between β_{max} results of the current experiment and those predicted by the two models might be due to differences in the nature and properties of the impact surfaces used in the experiments from which the above models were derived. Also, differences might arise due to simplifications used in deriving those models as well as due to errors associated with the corresponding experiments.

The Scheller-Bousfield model for predicting β_{max} was derived by approximating the flow in a drop impact by the squeeze flow of a cylindrical liquid column between two parallel plates. The correlation is expressed as:

$$\beta_{max} = 0.91 \, (Re^2 Oh)^{0.133}$$

As was shown in Figure 4.1, the spread factors predicted by this model for the conditions in the current experiments are nearly 15% lower than the actual experimental results. However, since the trends of the two results are similar, it might be possible to introduce a small correction in the Scheller-Bousfield model for a more accurate estimate of β_{max}. It was found that if the index of $Re^2 Oh$ is increased from 0.133 to 0.146, the

resulting correlation can predict β_{max} to within 5% of the experimental results as shown in Figure 4.2. Thus, the modified correlation for maximum spread factor can be written as:

$$\beta_{max} = 0.91\,(Re^2 Oh)^{0.146}$$

It can be seen that the correlation given by Scheller and Bousfield predicts lower values of maximum spread factors compared to the experimental results.
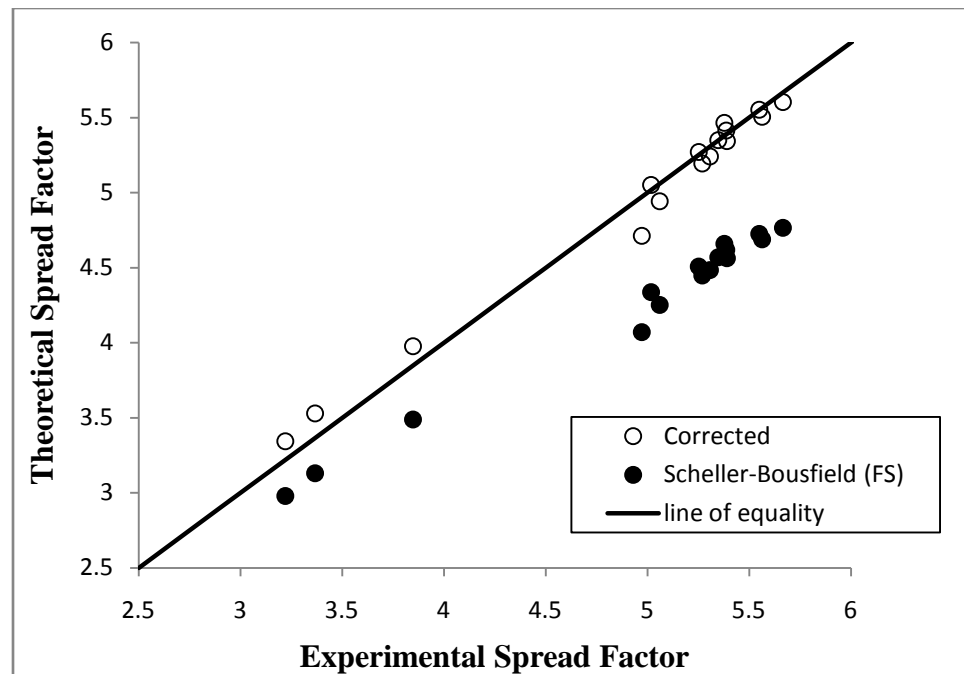

Figure 4.2: Comparison of modified correlation for β_{max} with experimental results

4.1 Splashing Threshold of Pure Liquids

Ethanol and methanol were used as the test liquids for splash ratio tests. Splash points for ethanol drops were obtained up to a pressure of 7.2 bars while for methanol, data points could be obtained only up to 3.5 bars, beyond which excessive distortion of the drops occurred. Reynolds Number, based on equivalent drop diameter and the impact speed, varied from 5000 – 8500 for methanol while for ethanol it was in the range of

2300 – 3200. Hence, the regime of interest was completely different than the tests by Xu et al. where the Reynolds number values were much higher due to bigger drop sizes and higher impact speeds. The current tests were in a regime well below the critical speed region as mentioned by Xu et al. [1]. Figure 4.2 shows a sequence of images of an ethanol drop under two different pressures, highlighting the determination of the threshold pressure, P_T.
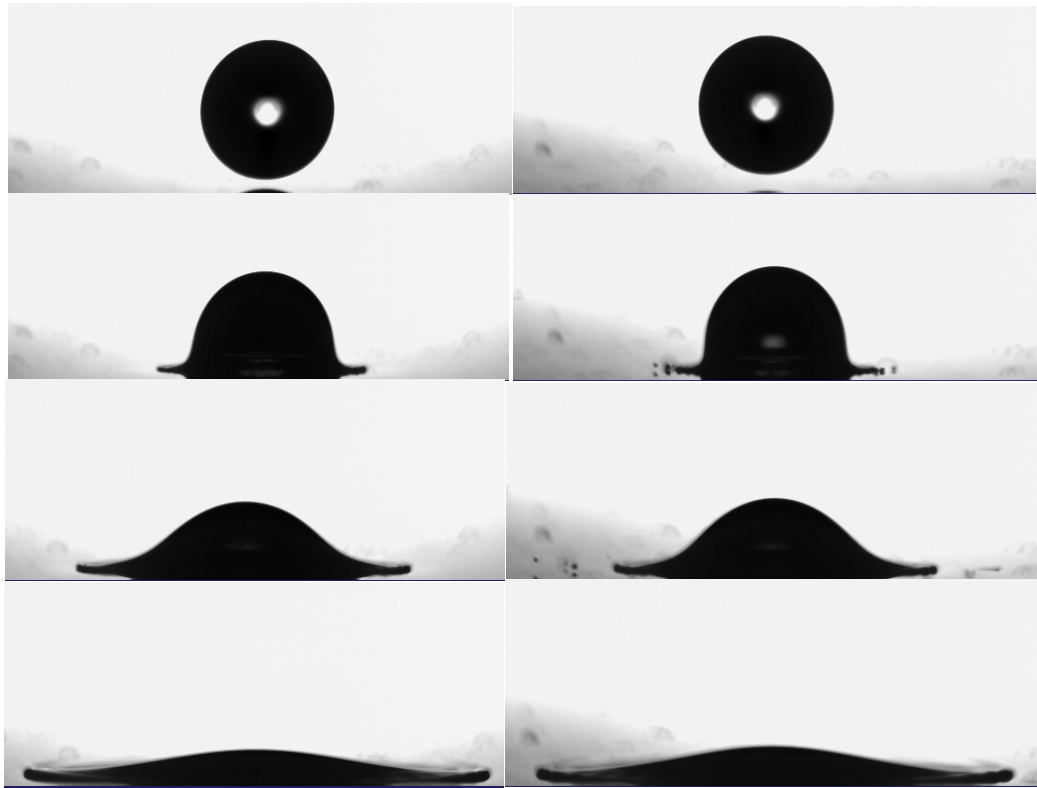

Figure 4.3: Impact of ethanol drop at different chamber pressures. (a) At 1.4 bars no splash occurs. (b) At 1.55 bars, tiny droplets are ejected all around; 1.55 bars is the threshold pressure at 2.15 m/s

A plot of threshold pressure vs. impact speed for the two liquids is shown in Figure 4.4. As can be seen, the threshold pressure increases sharply towards lower impact speeds which means that much higher pressures are required to induce splashing at low

drop sizes or drop speeds. The splash ratio as calculated using expression (1) in chapter 2, correspondingly increases rapidly towards lower impact speeds as shown in Figure 4.5. A power law curve could be fitted to the different splash points obtained:

$$\frac{\Sigma_G}{\Sigma_L} = C * V_0^{-m}$$

where, *C* and *m* are constants depending on the liquid. This is unlike the results of Xu et al., who found the splashing ratio to be constant at 0.45 in the regime of impact speeds above a critical value, which varied with the liquid. In both figures, the slope of the curves can be seen decreasing with increasing impact speed. Following this decreasing trend from Figure 4.5, we can expect the splash ratio to approach a value of 0.45 at higher impact speeds and correspondingly lower threshold pressures. Also, from Figure 4.4, since the slope of the curve is decreasing, beyond the critical speed, threshold pressure can be expected to decrease more gently with speed, as observed by Xu et al. and shown in Figure 2.1 (b). Thus, the current data should approach the results of Xu et al. at high speeds, giving a more general description of splashing condition. Hence, we have two regimes with different behavior of the splash ratio – first regime beyond critical speed where splashing ratio is a constant while the second regime below the critical speed where the splashing ratio increases sharply. Around the critical speed, transition takes place through a non-monotonic behavior of the splash ratio. At lower impact speeds, the high values of threshold pressure, and much higher change in its value compared to relatively small changes in impact speed, suggest that compared to chamber pressure, impact speed and hence the kinetic energy is more important factor in determining drop splashing. A drop hitting a smooth surface at higher speed in a low chamber pressure condition would be more likely to splash than a drop with lower impact speed and proportionately higher surrounding pressure.
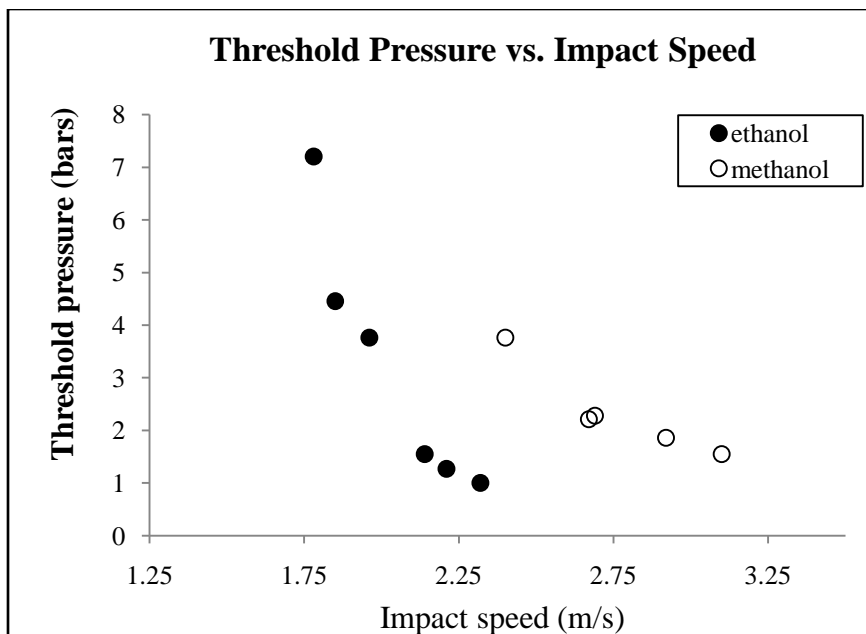
Figure 4.4: Threshold pressure vs. impact speed for ethanol and methanol
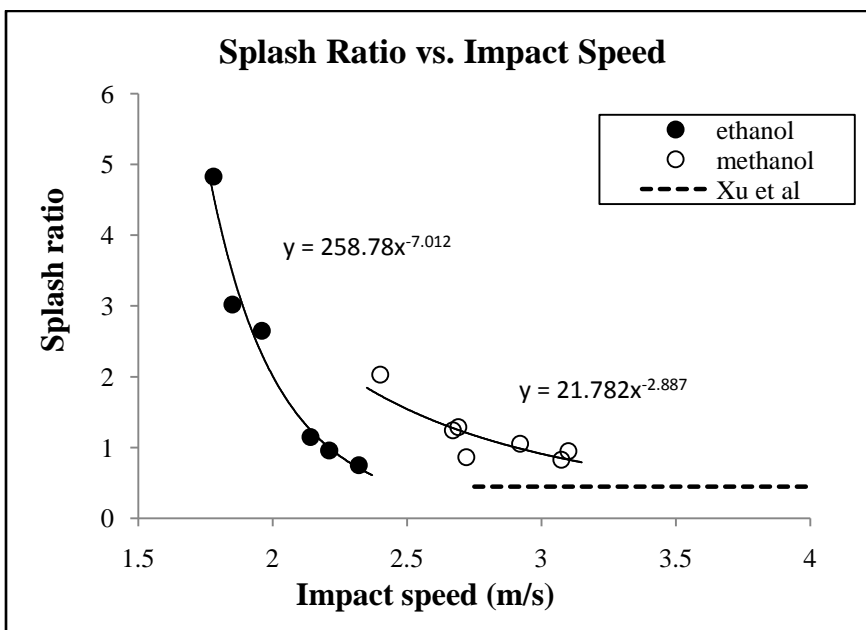

Figure 4.5: Splash ratio vs. impact speed for ethanol and methanol

Combining the results from present tests with the findings of Xu et al., it might be possible to chart the behavior of splash ratio over a more complete range of impact Reynolds numbers as shown in Figure 4.6. As stated earlier, the current results seem to approach those of Xu at high impact speeds. We can also see that methanol splashes at higher Reynolds numbers than ethanol which means that for same drop size and threshold chamber pressure, impact speed needed for methanol splash is higher. This is consistent with previously known results that within a certain range of viscosity, higher viscosity liquids tend to splash easily compared to low viscosity liquids. It is seen that the threshold pressure and splash ratio curves in Figures 4.4 and 4.5 for methanol and ethanol do not collapse on each other unlike the high impact speed results of Xu et al. [1]
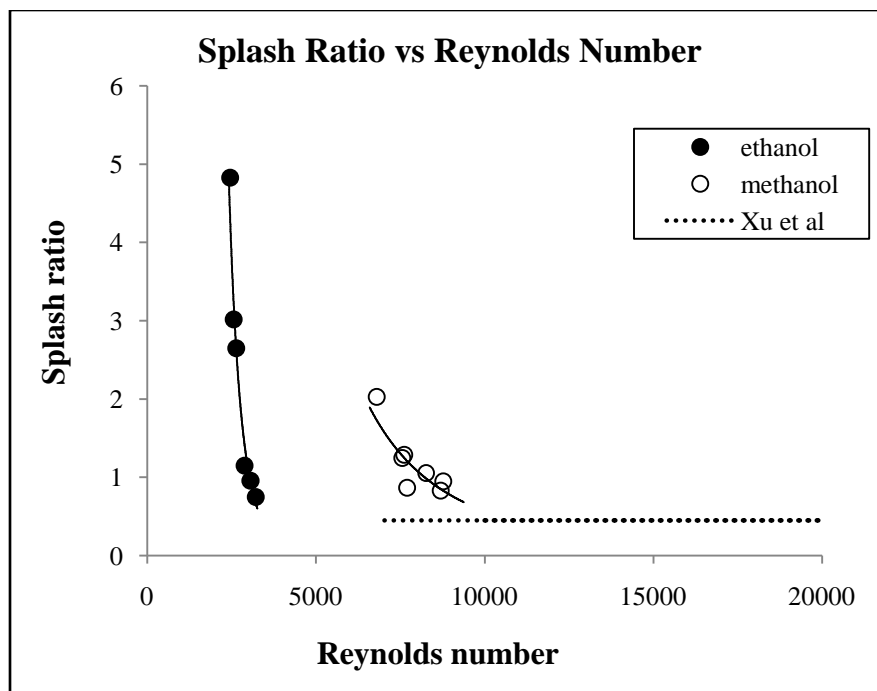

Figure 4.6: Values of splash ratio in different regimes based on Reynolds number

Figure 4.7 shows a plot of the splashing ratio with chamber pressure. Splashing ratio is seen to increase almost linearly with pressure, a result which was also noted by Dix et al. [2], as mentioned in earlier chapters. He concluded this to be a distinct and general behavior at high pressures, different than that observed at low pressures by Xu et al. But, the current study makes it clear that, the linear increase of splash ratio with pressure is a natural and expected result because the change in impact speeds for splashing at different pressures is relatively small, and hence the value of splashing ratio is mainly determined by the pressure term in expression (1), which is linear. This result, however, supports the idea that impact speed plays a more important role in determining splash of a drop since, even with a small change in impact speed, the pressures needed to induce splashing are much higher. Dix et al. also perhaps overlooked the fact that the regime of their tests was completely different than those of Xu et al. Thus, results of the
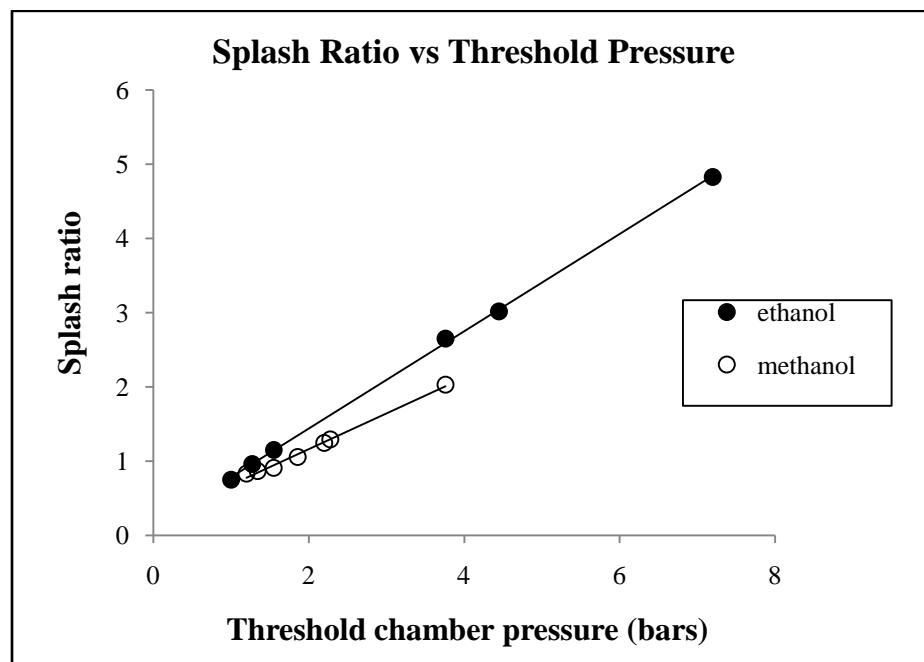

Figure 4.7: Variation of Splash ratio with threshold pressure

present study characterize the behavior of splash ratio in relatively lower drop inertia region and improve upon the conclusions made by Dix et al.

An interesting feature observed about splashing drops was that, even under similar conditions of pressure, impact speed and size, drops that were prolate prior to impact were less prone to splashing than the ones that were oblate. This is shown in Figure 4.8. In terms of radius of curvature, the oblate drops had a lower curvature, while the prolate ones had a higher curvature on the impacting side. This effect of drop shape on splashing was also reported by Stow and Hadfield in his experiments with water drops. However he considered that as an error source and didn't offer any explanations for that observation.
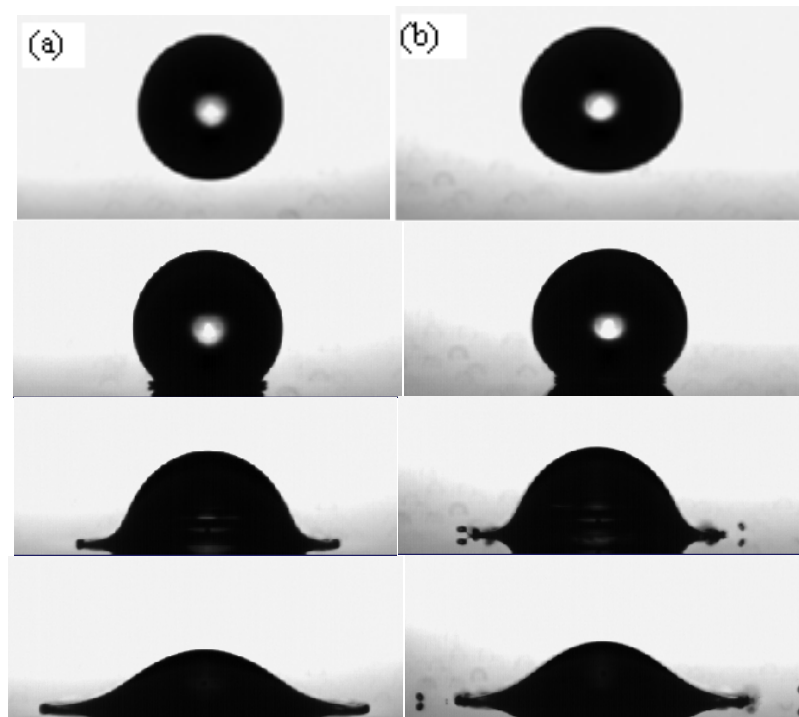

Figure 4.8: Impact of two ethanol drops at 5.14 bars, 1.82 m/s
(a) spherical drop shows no splash; (b) oblate drop splashes

There can be two possible explanations for this observation. First, a lower curvature of the point of impact on the drop means that a larger drop area comes in contact with the surface upon initial impact. This would generate compression waves at multiple points leading to a strong wave that travels back into the drop. A sufficiently strong wave can then cause droplet ejection at the advancing contact line immediately after impact. In case of a drop with high curvature impact, the displacement wave is initiated at fewer points and perhaps doesn't have sufficient strength to cause splashing.

A second line of reasoning points to the role of air entrainment in drop splashing. As the drop approaches the surface, air trapped between the drop and the surface is compressed. As shown in Figure 4.9, in case of an oblate drop, the compressed air has a narrow channel to escape and hence gets further compressed. As this compressed air tries to escape just before impact, it entrains the liquid and ejects secondary droplets upon impact. On the other hand, for a high curvature drop, there is a wider space available for the air to escape. The air is less compressed and can escape freely. Such air entrainment has been cited by Jepsen et al. [30] as a possible cause of splashing. Numerical simulations using Fluent, of a drop impacting a solid surface, have shown that, very close to the instant of impact, the air between the drop and the surface, gets accelerated to speeds around ten times the impact speed. This accelerating air could cause instabilities in the liquid near the impact point which grow, resulting in droplet ejection. Based on such studies, Jepsen et al. suggested Kelvin-Helmholtz to be the instability mechanism rather than the Rayleigh-Taylor instability. The effect of shape on splashing, as noted in this work, certainly supports that theory.

The fact that splashing is affected by drop shapes can be used to give a more realistic input to numerical models simulating splashes and sprays. Further investigations could be carried out to investigate the possibility of existence of a critical curvature of the drop that might result in splashing under a given set of conditions.
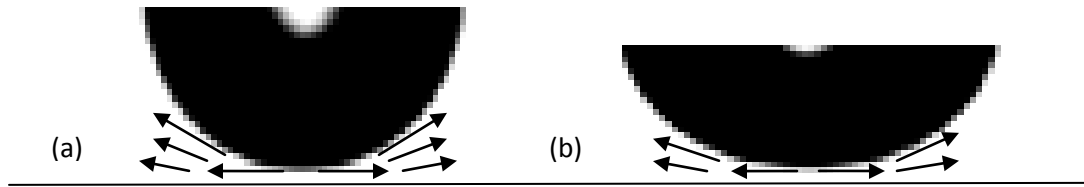
Figure 4.9: Air movement near the point of impact (a) Wider channel for air movement under a prolate drop (b) Narrower channel under an oblate drop.

4.2 Spreading of Liquids

Spreading of liquid drops was studied up to a chamber pressure of 12 bars for impact speeds well below the splashing regime. Since surrounding gas pressure exerts a restraining force on the advancing liquid-solid contact line, variations in the maximum spread factor β_{max}, with pressure was considered an interesting case for study. All the models proposed so far for predicting β_{max} consider it to depend on liquid properties, impact speed, drop size and contact angle. A direct influence of chamber pressure on spread factor has seemingly not been examined.

As explained earlier, four different liquids were tested using two different methods owing to the nature of liquids and set-up limitations. Cetane, propanol and diesel were tested by releasing drops from a constant needle height at different chamber pressures. Figure 4.10 shows a comparison of β_{max} obtained at high pressures to those at atmospheric pressure, keeping impact speeds similar for the two cases as explained in chapter 3. Solid lines represent drop impacts at high chamber pressures from a constant needle height. The curve slopes downwards because the impact speed goes on decreasing with pressure due to increased drag on the falling drop. The dotted lines show the spread factors obtained at 1 bar for impact speeds equal to the respective high pressure tests. For all three liquids, it can be seen that both the curves follow similar decreasing trend over the entire pressure range. There is a small difference between the two curves which could be attributed to factors like slight variabilities in drop size, drop spin or vibration, etc. that

might occur at higher pressures. Should pressure effect spreading, the curves could be expected to follow different trends. However, the fact that the two curves don't diverge at all suggests that pressure doesn't affect spread factor of the liquids tested, in the range of applied chamber pressures.
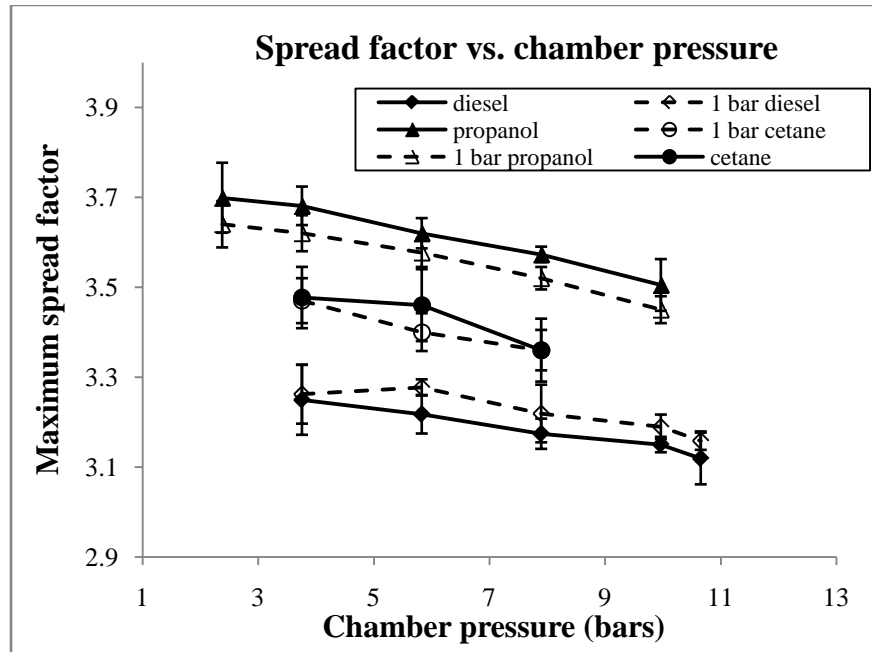

Figure 4.10: Maximum spread factor vs. chamber pressure for drop impacts from constant needle height.

However, from Figure 4.11 we can see that for ethanol, the spread factor shows an increase of about 3% in going from 1 bar to 7.2 bars. This behavior is different from that observed for other liquids and a bit counterintuitive. No significant change in drop sizes was noticed in this range of pressures for ethanol. A possible contribution to this behavior may be due to a relatively higher decrease in surface tension of ethanol (1.5% approx.) than the increase in its viscosity (0.5% approx.) in the range of 1 bar to 10 bars. Figure 4.12 shows the behavior of surface tension and viscosity of ethanol with pressure,
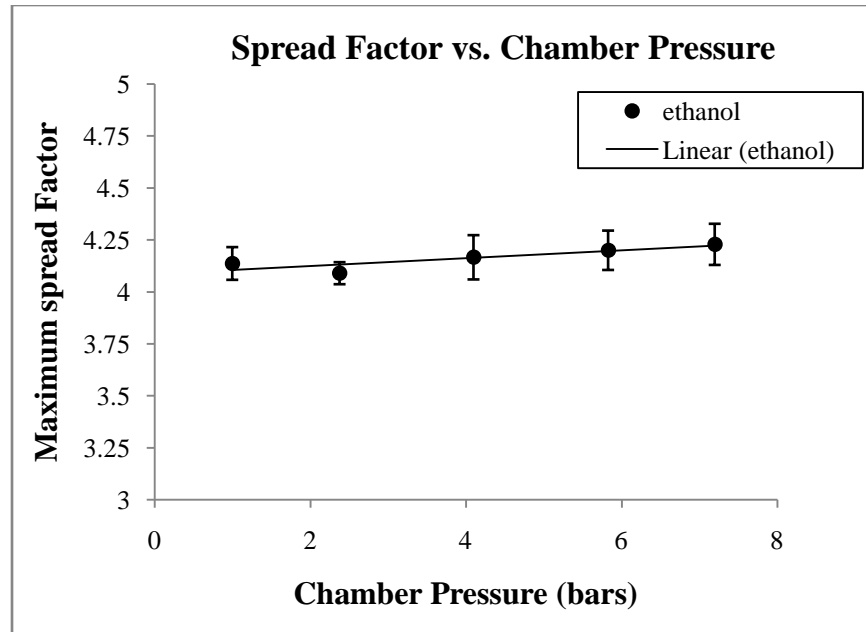
Figure 4.11: Spread factor of ethanol drops for $V_0 = 1.75$ m/s

in a surrounding of Nitrogen. Reduction in surface tension should increase the spread factor while higher viscosity should limit it. Since the change in surface tension is higher than viscosity, ethanol shows a slight increase in β_{max}. On the other hand, for diesel the surface tension changes by about 3% in the same pressure range. However, the viscosity of diesel (~3.6 mPa-s) is much higher than that of ethanol which perhaps nullifies the effect of reduction in surface tension. The viscosity values of n-propanol and n-hexadecane are also comparable to diesel and hence these liquids do not show any change of spread factor from atmospheric to the highest chamber pressures used. It can thus be concluded that pressure does not directly affect drop spread; the liquid properties might change at significantly higher pressures resulting in a change in maximum spread factor.

A further confirmation of this independence of spread factor from pressure is suggested by studying the rate of increase of spread diameter with time at two different chamber pressures. Figure 4.13 shows a plot of the evolution of spread factor with non-dimensional spread time for two ethanol drops at 1 bar and 5.76 bars respectively. This
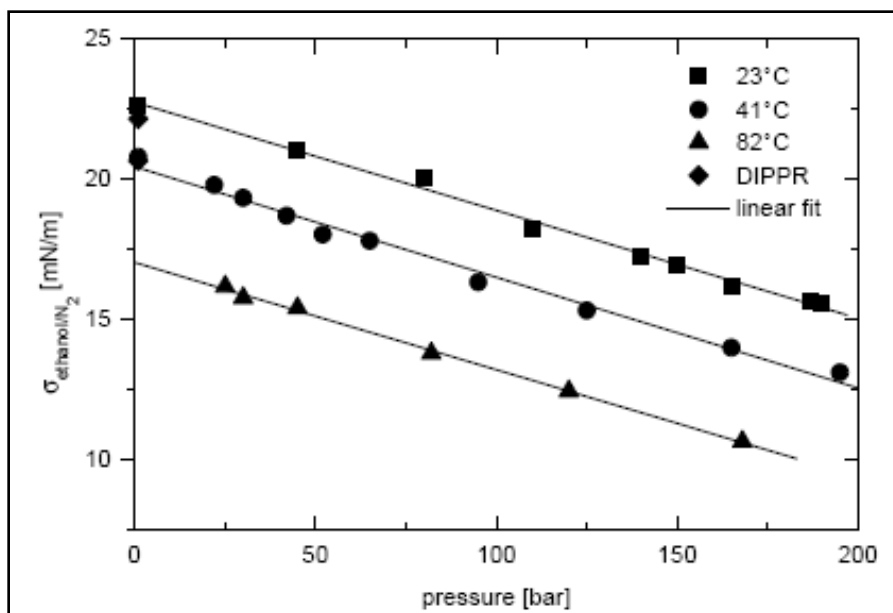
Figure 4.12: Interfacial tension of ethanol in contact with nitrogen as a function of pressure at different temperatures. [35]
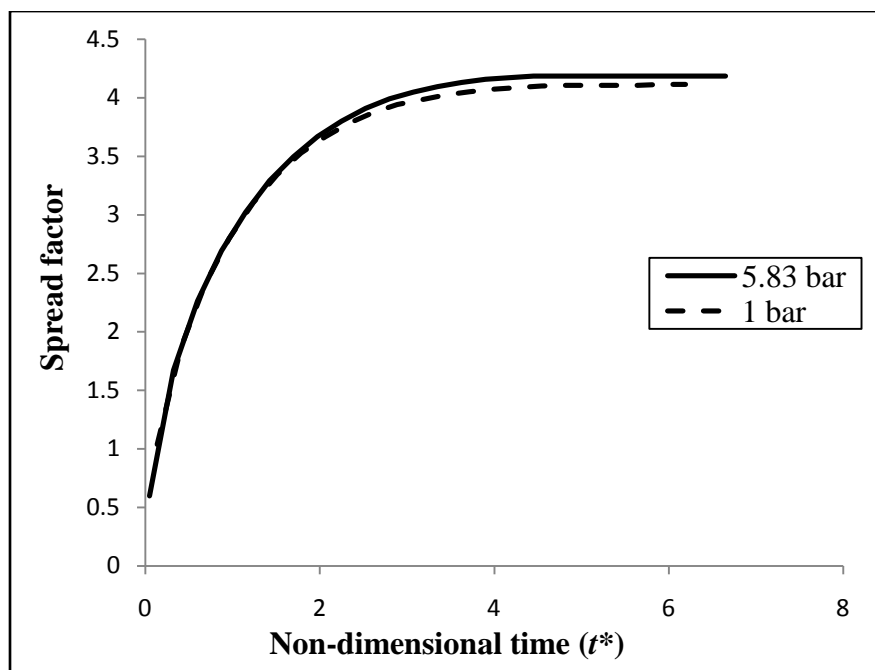

Figure 4.13: Spread factor vs. non-dimensional spread time for two ethanol drops at 1 bar and 5.83 bars respectively, at $V_0 = 1.75$ m/s.

temporal evolution of a drop deformation is obtained by measuring spread diameter (hence spread factor) at each time instant and plotting it against a non-dimensional time, given as $t^* = (t * V_0)/D_{eq}$ where, t is the total time from the instant of the frame just prior to impact. As can be seen, spread factor increases at almost identical rates for the two drops and the time to achieve the maximum spread diameter is also identical. The difference seen between the two curves in the initial stages of spreading is because the instant of impact of the two drops were not exactly the same. The drop at 5.83 bars impacted a bit later than the drop at 1 bar giving it a slightly lower spread factor in the initial stage. Beyond that, the two curves almost overlap before diverging near the maximum spread diameter. The drop at 5.83 bars has a higher maximum spread factor as explained earlier. Thus, Figure 4.13 clearly suggests that pressure does not affect the rate of drop deformation process.

CHAPTER 5
IMPACT OF NON-NEWTONIAN LIQUID DROPS

A wide range of industrial liquids fall under the category of non-Newtonian fluids which exhibit unique properties like shear-dependent viscosity, visco-elasticity, etc. Considerable amount of research has focused on studying the effect of these distinct properties in impacts of drops of different non-Newtonian liquids and understand the differences compared to the impacts of Newtonian drops. In the present study, drops of a blend of diesel and a high molecular weight polymer have been tested below the splashing regime. Addition of such long-chained polymers generally imparts shear-thinning properties to an originally Newtonian liquid. Since a drop impact process involves high shear rates, effects of non-Newtonian viscosity may be manifested in the form of relatively higher contact line speeds and greater spread diameters compared to a Newtonian liquid, under similar impact conditions. The present work was aimed at testing this premise to identify regions in drop spreading where viscosity differences become important. Salient features of the experiment are described below followed by a discussion on results.

5.1 Experimental Considerations and Procedure

For this experiment, Poly-butadiene 140 ND (Molecular weight$\approx$ 300000) was blended in diesel at four different concentrations using a magnetic stir bar. The concentrations used were 0.5%, 1.0%, 1.4% and 2.0% of polymer in diesel, by weight. It was observed that with increasing concentration, the base viscosity of the solution increased significantly. Drops of these blends were then tested under atmospheric pressure at three different impact speeds – 0.7 m/s, 1.2 m/s and 1.6 m/s, using a procedure similar to that mentioned in chapter 3. Frame speeds as high as 23000 fps were used for an accurate measure of spread diameters and average velocities of the contact

line. However, since base viscosities of the blends were significantly different from each other, a comparison amongst the impact results of these diesel-polymer blends would not yield meaningful results. Therefore, these non-Newtonian drops were compared to drops of a Newtonian mixture with correspondingly similar base viscosities. Since viscosity of a Newtonian liquid remains constant, while it changes with shear stress for a non-Newtonian liquid, such a comparison is expected to reveal the differences between the two cases. The Newtonian blends were prepared by mixing 99.8% pure glycerol in iso-butanol, at different concentrations. Viscosities were measured using a Brookfield Cup and Cone type viscometer as described in the following section. Iso-butanol was chosen as the solvent since its properties are similar to diesel, as shown in Table 3.1, and glycerol is readily soluble in it. The Newtonian drops were tested under same conditions as the polymer blends and then comparisons were made between the two types of blends for each corresponding concentration.

5.1.1 Viscosity Measurements

Viscosities were measured using a LV-series DV-II Brookfield Cup and Cone type digital viscometer. As the name suggests, the viscometer mainly consisted of a cup with a flat surface, and a cone which could be rotated at six different constant speeds using a synchronous motor. The working principle of such a viscometer states that when a test liquid is sheared between a cone with small θ, as shown in Figure 5.1, and a plate, at a constant angular speed, the fluid experiences a uniform shearing stress in all regions. The ratio of this shear stress to the strain rate gives the viscosity of the liquid at that shear stress. Shear stress acting on the cone is measured in terms of the total torque, M, acting on a beryllium-copper spring connected to the shaft rotating the cone. Relevant formula for the calculation of shear stresses, strain rate and viscosity are mentioned below.
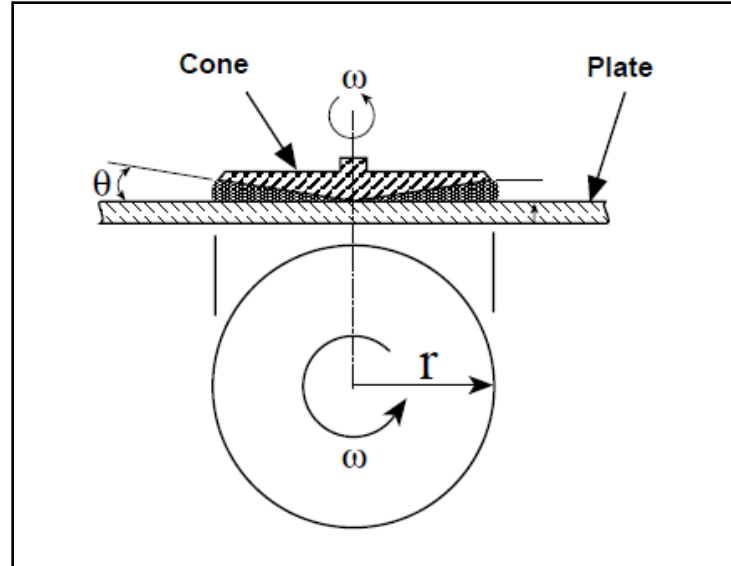
Figure 5.1: Schematic representation of a cup and cone viscometer operation

$$\dot{\gamma}\ (s^{-1}) =\ \omega/\sin\theta, \qquad \tau\ (dyn/cm^2) =\ M/\left(\frac{2}{3}\pi r^3\right), \qquad \mu(\text{Poise}) = \tau/\dot{\gamma}$$

The viscometer was first calibrated using a standard liquid whose viscosity was known at room temperature. Calibration was done to within 1% of the specified value. After calibration, viscosities of all samples of the diesel-polymer blend were measured. Viscosity values could be directly read from the digital display. The viscometer could measure accurately between 10% - 100% of the maximum torque capacity of the spring. Due to this, for a given composition, it was possible to measure viscosities only at 3 angular speeds. Once a measurement was complete, plots, of viscosity versus strain rate, as shown in Figure 5.2, were generated to which power law curves were fitted as best fit curves. The coefficient in the power-law equation of the curve was taken as the "zero-shear" or base viscosity of that sample. A Newtonian liquid was then prepared with a matching base viscosity.

A plot of the variation of viscosity with glycerol concentration for glycerol/iso-butanol mixtures was generated as shown in Figure 5.3 and was used to arrive at the
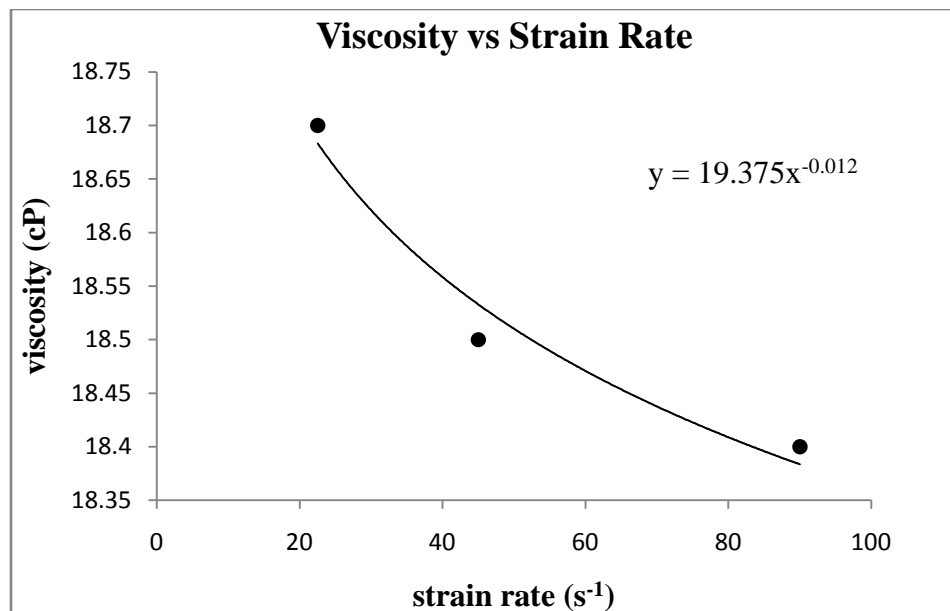
Figure 5.2: Viscosity vs. strain rate for 1.4% polymer in diesel. Base viscosity is given by the coefficient of the fit, $\mu_0 = 19.375$ cP, n = 1.012
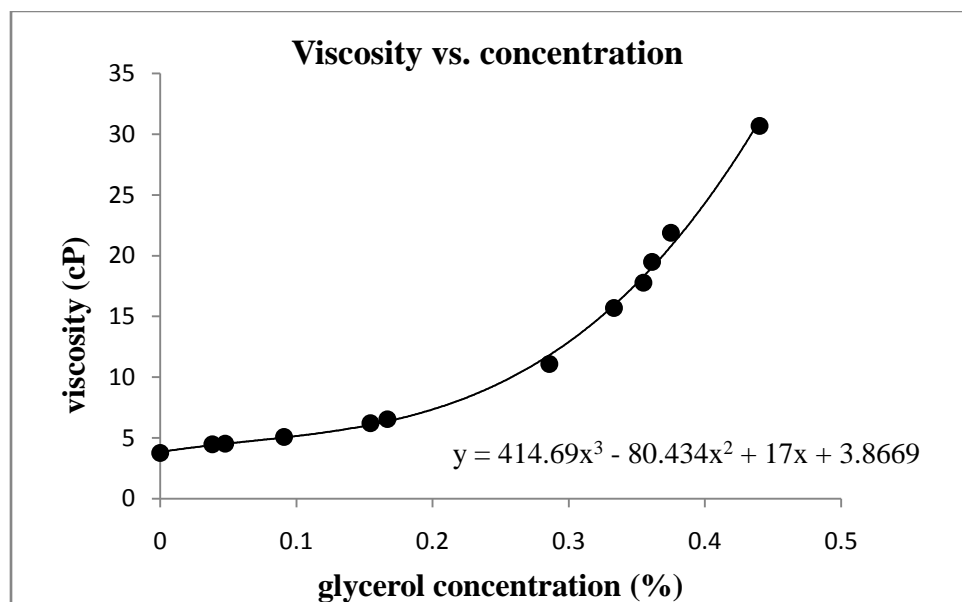

Figure 5.3: Variation of viscosity of glycerol-isobutanol blend with glycerol %

approximate concentrations of glycerol required to a desired viscosity value. Through further trial and error, glycerol concentrations to obtain Newtonian viscosities close to the base viscosity values of the polymer-diesel blend, were arrived at. Table 5.1 lists the different concentrations and their measured viscosities for both types of liquids.

Table 5.1: Concentrations and viscosities of the liquid blends

Polymer in diesel (Concentration %)	Base viscosity (cP)	Glycerol in iso-butanol (Concentration %)	Viscosity (cP)
0.5	4.33	3.8	4.44
1.0	6.1	14.53	6.23
1.4	19.375	36.1	19.5
2.0	39.3	47.1	39.6

5.2 Results

As mentioned previously and shown in Table 5.1, the base viscosities of the diesel-polymer blend increased by about ten times from the lowest to the highest concentration of the polymer. Also, it was noted that even with the same needle size, an increase of about 8% occurred in drop size with increasing concentration from 0.5% to 2.0% polymer. This increase could be attributed to the visco-elastic properties associated with the polymers, a fact that has been mentioned in published works on impact of non-Newtonian drops. A plot of the variation of β_{max} with impact speed for all the concentrations is shown in Figure 5.4. As can be seen, β_{max} decreases with increasing concentrations of the polymer. This behavior is expected due to the increasing viscosity of the blends. For each concentration, β_{max} increases with increasing impact speed, due to increasing kinetic energy of the impacting drops.

An indication of the effect of liquid properties like viscosity, on drop spreading, can also be obtained by examining the rate of spreading or the contact line speed. For a
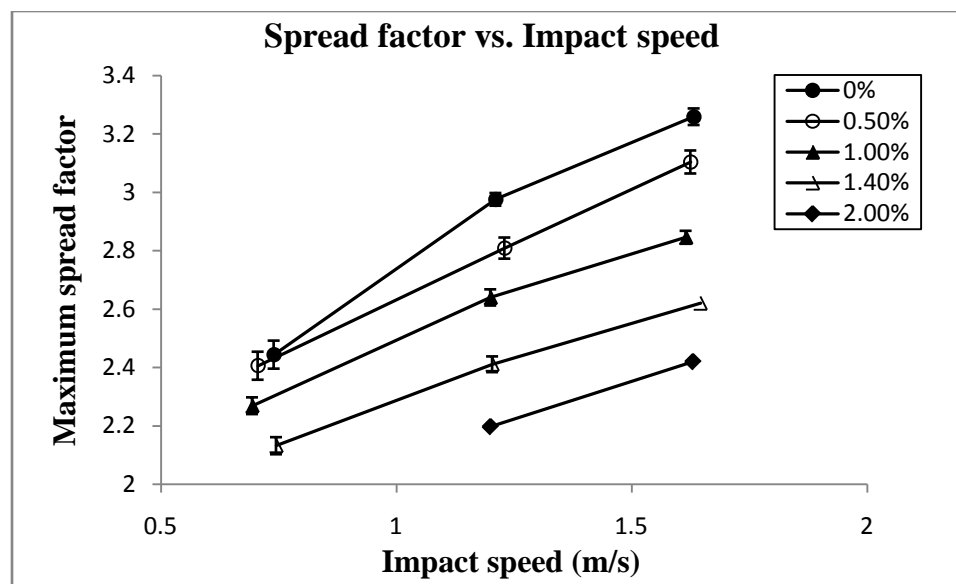
Figure 5.4: Maximum spread factor vs. impact speed for different polymer concentrations.

given drop size and impact speed, the greater the viscosity, the lower the rate of spreading should be, due to viscous damping. A plot of the average spreading velocities for diesel drops (D_{eq} = 2.15 mm) at two different impact speeds is shown in Figure 5.5. It can be seen that the spreading velocities for the drop with a higher impact speed (V_0 = 1.6 m/s) are greater than the one with a lower impact speed (V_0 = 0.7 m/s). For both drops, spreading velocities are significantly higher than the impact speed in the initial stages of drop spreading. However, the spreading velocities quickly reduce to the order of impact speed due to viscous effects. From Figure 5.5, it can be seen that the variation of the spreading velocities can be described by a power-law curve. Similar results about contact line speeds have been reported by Engel [12] and Jepsen et al. [30].

As was seen before, the addition of polymers to diesel resulted in a significant increase in the viscosity of the blend. This increase in viscosity caused a decrease of maximum spread factors for blends with higher concentration of polymer. A plot showing the variation of non-dimensional spreading velocity with non-dimensional time is shown in Figure 5.6 for two blends with polymer concentrations of 1% and 2%. The
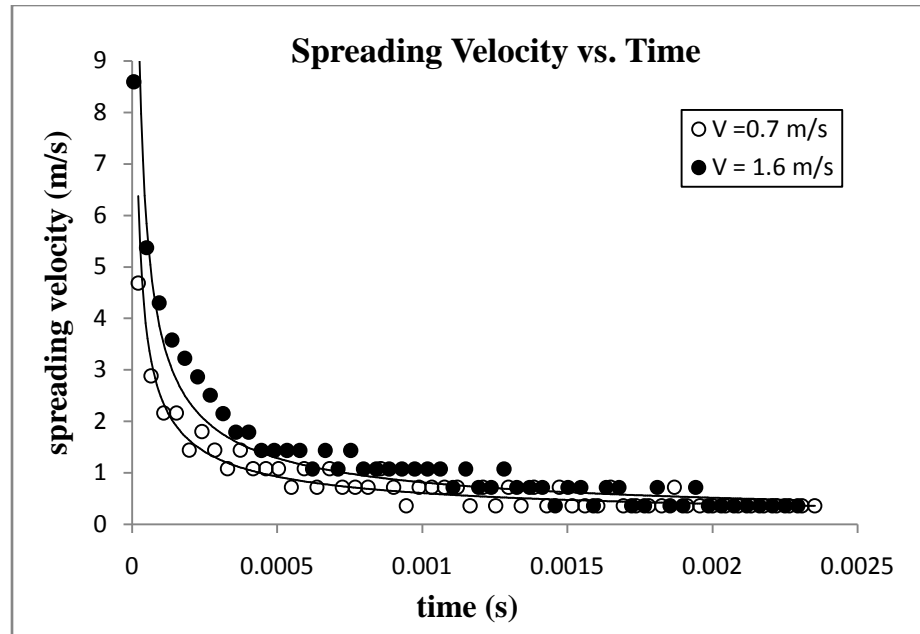
Figure 5.5: Variation of spreading velocities with time for two diesel drops with D_{eq} = 2.15 mm
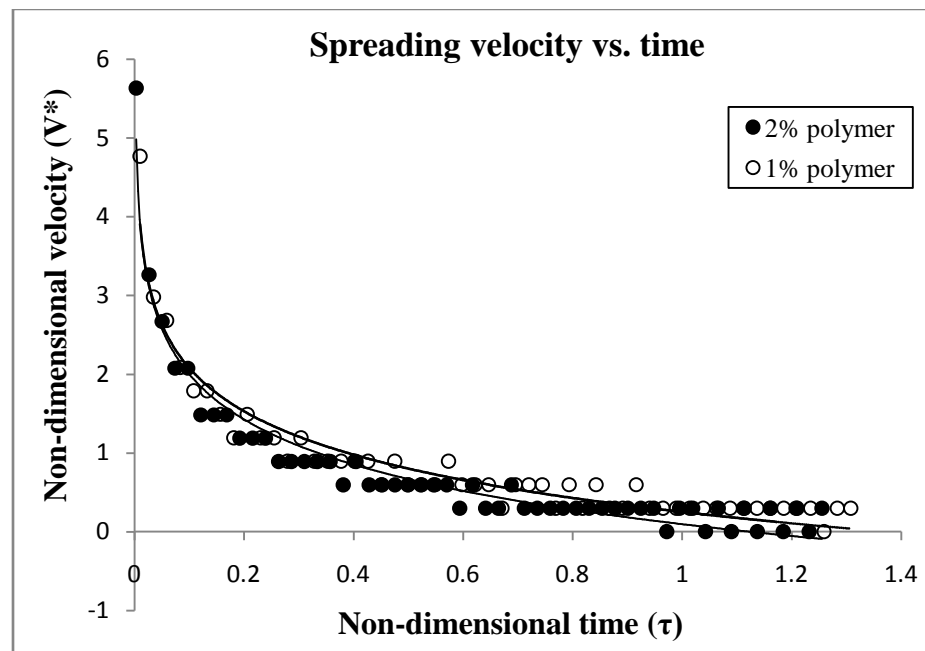

Figure 5.6: Non-dimensional average spreading velocities vs. non-dimensional spread time for two polymer concentrations

impact speeds for all the cases were nearly 1.2 m/s, while the drop diameters varied between 2.15 – 2.28 mm.

The data points for spreading velocities in both Figure 5.5 and Figure 5.6 show a step-like variation with time for each liquid, especially for $t^* > 0.2$. This is because the calculations for spreading velocities were done using discrete frames, separated by a definite time interval. Thus, the minimum resolution for the measurement of speeds corresponded to one camera frame; any change lower than that could not be measured. This resulted in an uncertainty of nearly 0.1 m/s in speed measurements. Considering these uncertainties, it can be concluded from Figure 5.6 that the spreading velocities are higher for the blend with 1% polymer concentration. This is due to the fact that the 1% solution had a lower base viscosity compared to the 2% solution. The interesting thing to note is that, for spread time $t^* < 0.1$, no difference is observed between the two cases, despite the significant difference in the liquid viscosities; however, the two trend lines start diverging for $t^* > 0.1$. This suggests that viscosity doesn't affect the drop deformation process in the earliest part of spreading. However, it retards the flow in 'spreading phase', i.e., for $t^* > 0.1$. This result is a further validation of the findings of Rioboo et al. [4], who suggested that spreading is independent of liquid and surface properties in the kinematic phase.

Thus, we see that the differences in viscosities of the test liquids are manifested in the behavior of contact line speeds and hence the spread factors. The above discussed results however, do not delineate the non-Newtonian effects, as the changes seen are due to the significant differences in base viscosities of the liquids tested. Therefore, as mentioned at the beginning of the chapter, the diesel-polymer blends were compared to Newtonian mixtures of glycerol and iso-butanol, having viscosities similar to the base viscosities of the diesel-polymer mixture. For nearly equal drop sizes and impact speeds, the differences between the two cases should be caused by the viscosity variation of the

non-Newtonian drops. Such a comparison would help in characterizing the non-Newtonian effects in such drops.

Figure 5.7 shows a comparison of the β_{max} values for diesel and pure iso-butanol at similar impact speeds. Due to the slightly lower surface tension of iso-butanol, the size of its drops was about 5% lower than those of diesel. The viscosities of the two liquids were nearly identical. It can be seen that, for similar impact speeds, the maximum spread factors for the two liquids are nearly identical. So, the spreading behavior of diesel and iso-butanol could be assumed reasonably similar. This ensures that, any change observed between the non-Newtonian and the Newtonian blends, is due to the addition of polymers and glycerol respectively, and not due to the parent liquids.
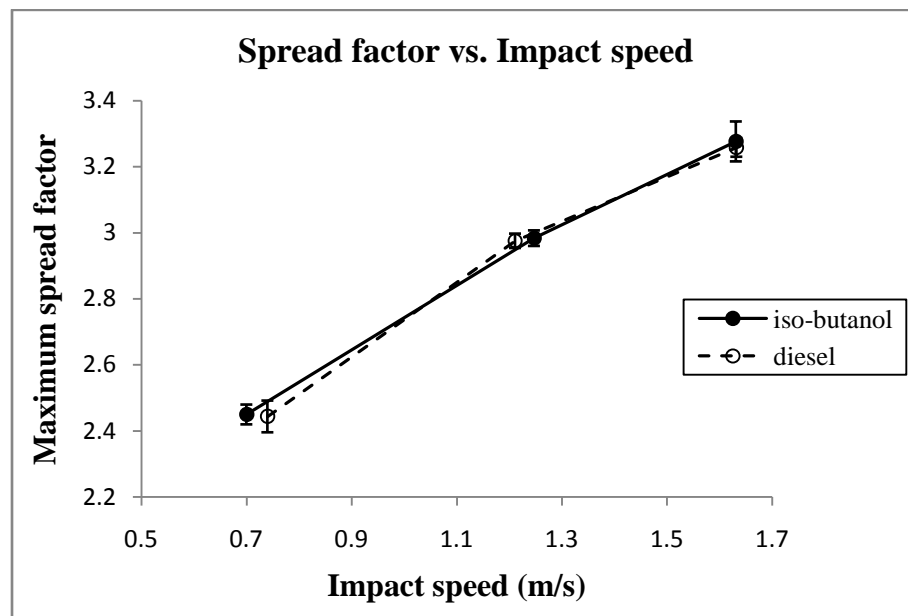

Figure 5.7: Maximum spread factor vs. speed for diesel and iso-butanol

The Newtonian mixtures were tested at similar impact speeds as the corresponding non-Newtonian blends and a comparison was made for the spread factors and spreading velocities. Figure 5.8 shows a comparison of β_{max} for 1.4% polymer in

diesel with the corresponding Newtonian blend, i.e., 36.1% glycerol in iso-butanol. It is seen that the spread factors for the glycerol-isobutanol mixture is about 8% lower than those for diesel-polymer blend. This might indicate that, as expected, the viscosity of the non-Newtonian drop reduces due to high strain rates during impact, which gives it a greater spread than the Newtonian drop, whose viscosity remains constant. However, the difference in drop sizes for the two kinds of liquids needs to be accounted while analyzing this result. It was observed that, for the same needle size, the average size of the drop for the glycerol-isobutanol mixture was around 2.00 mm, while, for the polymer-diesel blend, average drop sizes were nearly 2.25 mm. It is possible that this 11% decrease in drop size might have resulted in lower β_{max} for the Newtonian liquid. Also, the value of surface tension was not measured for the two kinds of liquid. A significant difference in the values of surface tensions can also contribute to variations in spread factors.

Figure 5.9 shows a comparison of the evolution of spread factors with non-dimensional time for the two mixtures. It can be seen that the final spread factor for diesel-polymer blend is greater than the glycerol-isobutanol mixture, as already shown in Figure 5.8. The two curves overlap in the initial part of spreading, i.e. for $t^* < 0.6$. After that, the rate of increase spread factors for diesel-polymer mixture decreases slightly compared to the glycerol-isobutanol mixture. The curve for the glycerol-isobutanol mixture shows a dip after reaching a maximum value. This dip is due to a rapid change of contact angle occurring at the maximum diameter, and a strong reflection wave that reduces the lamella diameter d_{lam} as shown in Figure 5.10. As was discussed earlier, d_{lam} was used to measure the spread factors rather than the contact line diameter d_{cont}. The final spread diameter was the diameter of the contact line at equilibrium. For the diesel-polymer drops, this change of contact angle was more gradual and hence no dip is observed in its curve. This difference in behavior of the two drops may be due to the possible difference in the surface tension of the two mixtures.
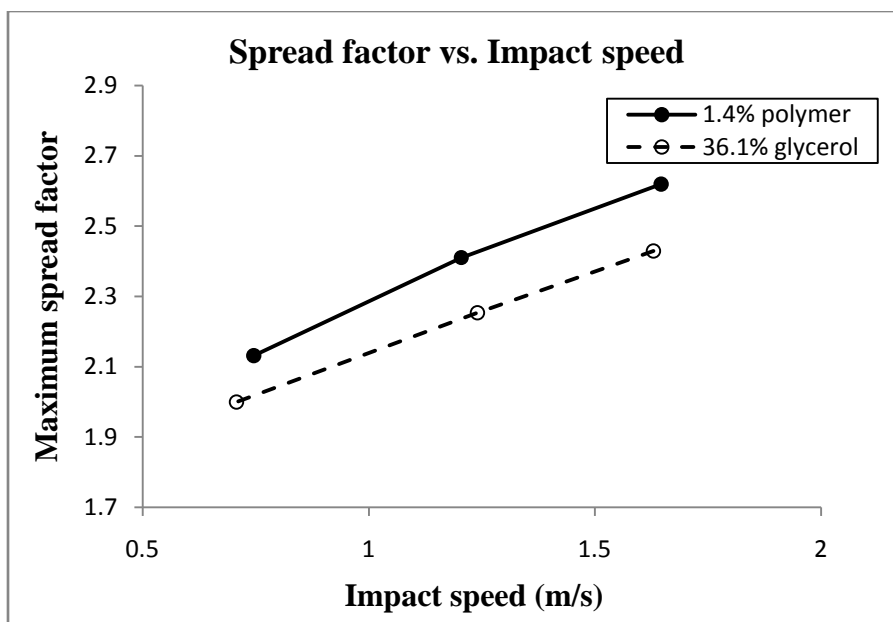
Figure 5.8: Comparison of maximum spread factor for 1.4% diesel-polymer blend and 36.1% glycerol-isobutanol mixture
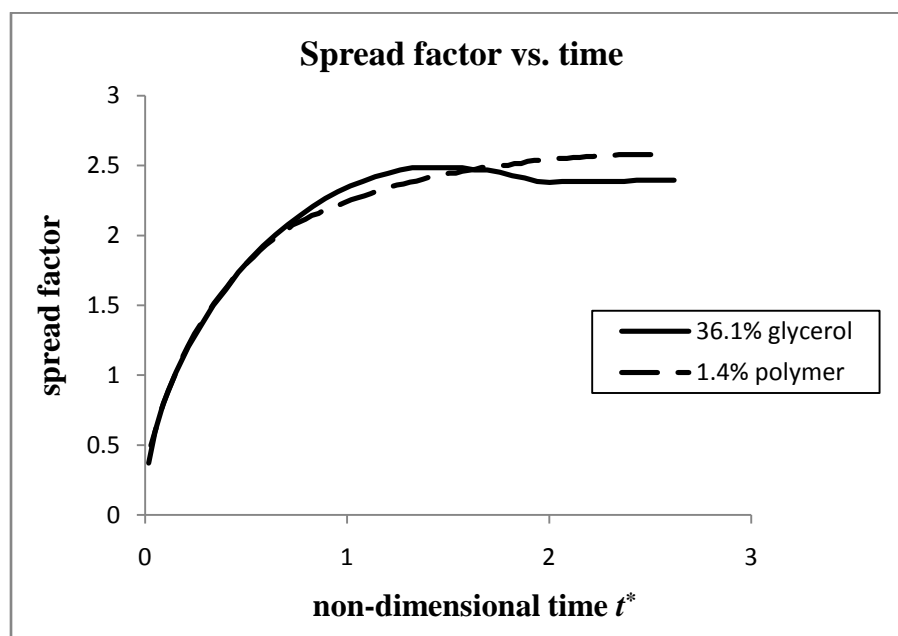

Figure 5.9: Evolution of spread factor with non-dimensional time for polymer-diesel and glycerol-isobutanol blends
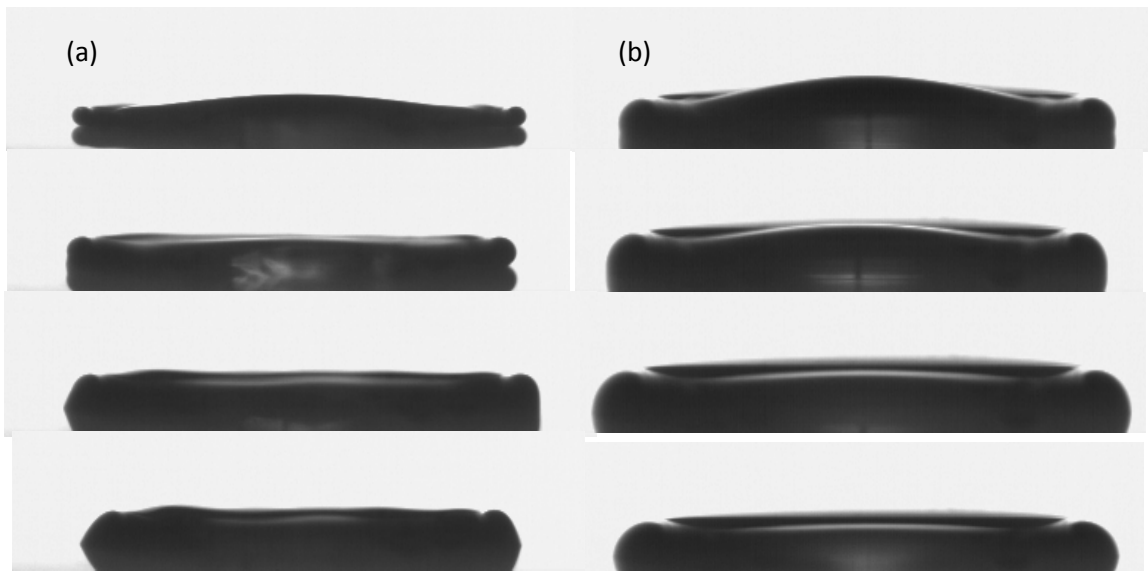
Figure 5.10 Spreading near the maximum diameter (a) glycerol-isobutanol blend (b) polymer-diesel blend

Finally, a comparison of the average spreading velocities for the two liquid blends is shown in Figure 5.11. It can be seen that the non-dimensional spreading velocities are similar for the two cases. Any effect of non-Newtonian viscosities is not evident from this velocity comparison. It is possible that such effects were suppressed due to the variation in drop sizes, and possibly, surface tension values between the Newtonian and the non-Newtonian liquids used. To capture the effects better, improved tests need to be carried out such that similar drop sizes and surface tension values are obtained. Also, higher molecular weight polymers could be used which might impart stronger non-Newtonian behavior to the parent liquid.
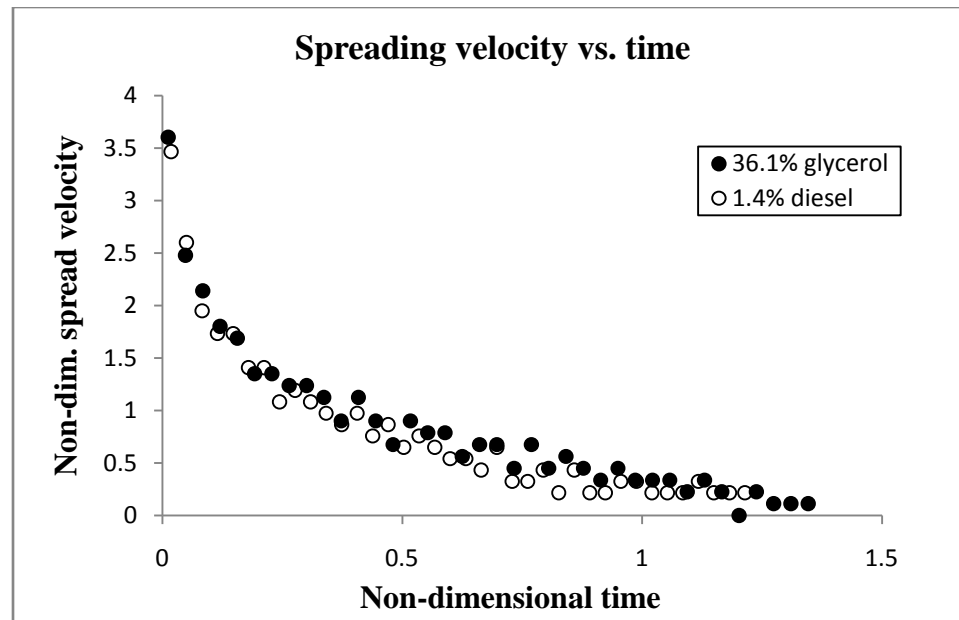
Figure 5.11: Comparison of variation of spreading velocities with time for the two liquid blends

Though this initial comparison between a non-Newtonian and a Newtonian blend could not lead to conclusive results about effects of variable viscosity in a drop spreading process, a possible methodology for the comparison of non-Newtonian drop impacts with the impacts of Newtonian drops has been introduced and established. It was shown through viscosity measurements that the addition of large weight polymers to Newtonian liquids, imparts non-Newtonian behavior to the parent liquid. Also, it was validated that the initial part of the drop spreading process is unaffected by properties of the liquid. Such a conclusion was also made by Rioboo et al. [4]

CHAPTER 6
CONCLUSIONS AND FUTURE WORK

Drop impact tests were carried out under high chamber pressures on a smooth and dry quartz surface using five different liquids to further study the effect of gas pressure on splashing and spreading behavior of liquid drops. Splashing tests were performed using ethanol and methanol in a regime below the critical speed mentioned by Xu et al. [1] in their tests. Drops roughly 2.1 mm and 2.7 mm in diameter and with impact speeds between 0.7 – 3.5 m/s were imaged using high speed photographic technology.

The free-spreading model given by Scheller and Bousfield [15] for predicting maximum spread factor was modified so that the resulting correlation could match the experimental results more accurately. This new correlation predicted β_{max} within 5% of the current experimental results. In splash tests, threshold pressure and splash ratio, as proposed by Xu et al., were found to increase sharply at low impact speeds suggesting that much higher pressures are required to induce splashing at low speeds. It could be concluded that drop kinetic energy is more vital for splashing compared to gas pressure. Splashing was found to be affected by drop shape or curvature. Surrounding air entrainment and stronger displacement waves could be possible explanations for this observation. Like the experiments of Xu et al., a higher viscosity liquid (ethanol) was found to splash more readily compared to a lower viscosity liquid (methanol). It was established that the observations of Dix et al. [2] about the non-occurrence of splashing even for a splash ratio of 3.5, were due to a regime change, and not a behavior caused due to high pressures.

In the range of pressures tested, spreading was found to be unaffected by chamber pressure. Spread factors for propanol, diesel and cetane didn't show significant deviation at high pressures from the values at atmospheric pressure. However, ethanol showed a slight increase of spread factors which probably could be due to a change of liquid

properties at higher pressures. It was concluded that pressure could affect spreading indirectly by changing liquid properties like surface tension.

Drop impact tests for a non-Newtonian mixture of a large molecular weight polymer and diesel in different concentrations validated some previously known results. It was shown that drop spreading in the initial stages ($t^* < 0.1$) is independent of liquid viscosity. The effect of viscosity on rate of spreading and spread factors was also shown for $t^* > 0.1$. It was seen that the average spreading speeds were greater for a low viscosity liquid. However, comparison with impacts of a Newtonian mixture of glycerol and iso-butanol did not yield conclusive results about effects of variable viscosities in drop impacts.

The present study has thus established a possible methodology to investigate an aspect of non-Newtonian drop impacts. Future research could follow this work by testing with polymers of much higher molecular weights which could impart stronger non-Newtonian characteristics. Suitable liquids and testing procedures could be chosen so that drop sizes and other properties like surface tension are similar for both kinds of liquids, which was a limitation in the current work. Better imaging techniques might be required for such tests for a more accurate measure of spreading parameters.

Further studies for quantifying the effect of drop curvature on splashing could be carried out. The data points collected in the current tests were limited due to the distortion of drops at high pressures. Better drop generators and other liquids could be used to investigate drop impacts at even higher pressures. Future tests could also look to continue the work on impact tests for drops of binary liquid mixtures, for which the initial tests were done by Karakaya et al. [3]. Such binary mixtures were not tested in the current experimental work. Such improved tests would certainly yield more insight into the drop deformation process.

REFERENCES

1. Xu, L., Zhang, W.W., Nagel, S.R., *"Drop splashing on a dry smooth surface",* Physical Review Letters, The American Physical Society, PRL 94/184505, 2005.

2. Dix, A., *"Pressure effects on drop impact with a smooth dry surface",* Master's thesis, University of Iowa, May 2007.

3. Karakaya, I., *"Assessment of pressure-induced viscosity variation through examination of drop impact",* Master's thesis, University of Iowa, June 2007.

4. Rioboo, R., Tropea, C., and Marengo, M., *"Outcomes from a drop impact on solid surfaces",* Atomization and sprays, Vol. 11, pp. 155-165, 2001

5. Dussan, E.B., *"On the spreading of liquids on solid surfaces: static and dynamic contact lines",* Annual Review of Fluid Mechanics, pp. 371-400, 1979

6. Chandra, S. and Avedisian, C.T., *"On the collision of a droplet with a solid surface",* Proceedings: Mathematical and Physical Sciences, Vol. 432, No. 1884, Jan. 1991.

7. Rein, M., *"Phenomena of liquid drop impact on solid and liquid surfaces",* The Japan Society of Fluid Mechanics, Fluid Dynamics Research 12, pp. 61-93, 1993.

8. Yarin, A.L., *"Drop impact dynamics: splashing, spreading, receding, bouncing",* Annual Review of Fluid Mechanics, Vol 38: 159-92, 2006.

9. Rioboo, R., Marengo, M., and Tropea, C., *"Time evolution of liquid drop impact onto solid, dry surfaces",* Experiments in Fluids 33, pp. 112-124, 2002.

10. Biance, A.L., Clanet, C., and Quere, D., *"First steps in the spreading of a liquid droplet",* The American Physical Society, Physical Review E 69, 016301, 2004

11. Sikalo, S., Marengo, M., Tropea, C., and Ganic, E.N., *"Analysis of impact of droplets on horizontal surfaces",* Experimental Thermal and Fluid Science, Vol. 25, pp. 503-510, 2002.

12. Engel, O.G., *"Water drop collisions with solid surfaces",* Journal of Research of the National Bureau Standards, Vol. 54, No. 5, May 1955.

13. Stow, C.D. and Hadfield, M.G., *"An experimental investigation of fluid flow resulting from the impact of a water drop with an unyielding dry surface"*, Proceedings of the Royal Society of London, Series A, Mathematical and Physical Sciences, Col. 373, No. 1755, 419-441, Jan. 1981

14. Pasandideh-Fard, M., Qiao, Y.M., and Mostaghimi, J., *"Capillary effects during droplet impact on a solid surface",* American Institue of Physics, Physics of Fluids 8(3), March 1996.

15. Scheller, B.L. and Bousfield, D.W., *"Newtonian drop impact with a solid surface",* Fluid mechanics and transport phenomena, American Society of chemical engineers, Vol. 41, No. 6, June 1995.

16. Elliott, G.E.P. and Riddiford, A.C., *"Dynamic contact angles",* Journal of Colloid Interface Science, 23, pp. 389-398, 1966.

17. Sikalo, S., Wilhelm, H.D., Roisman, I.V., Jakirlic, S. and Tropea, C., *"Dynamic contact angle of spreading droplets: Experiments and simulations",* American Institute of Physics, Physics of Fluids 17, 2005.

18. Cox, R.G., *"The dynamics of the spreading of liquids on a solid surface. Part 1. Viscous flow"*, Journal of Fluid Mechanics, Vol. 168, pp. 169-194, 1986.

19. Zhang X. and Basaran, O.A., *"Dynamic surface tension effects in impact of a drop with a solid surface",* Journal of Colloidal and Interface Science 187, 166-178, 1997.

20. Harlow, F.H. and Shanon, J.P., *"The splash of a liquid drop",* Journal of Applied Physics, Vol. 38, No. 10, pp. 3855-3866, 1967.

21. Fukai, J., Shiiba, Y., Yamamoto, T., Miyatake, O., Poulikakos, D., Megaridis, C.M., and Zhao, Z., *"Wetting effects on the spreading of a liquid droplet colliding with a flat surface: Experiment and modeling",* American Institute of Physics, Physics of Fluids 7(2), 1995

22. Bussman, M., Chandra, S. and Mostaghimi, J., *"Modeling the splash of a droplet impacting on a solid surface",* Physics of Fluids, American Institue of Physics, Vol. 12, No. 12, 2000

23. Roisman, I.V., Rioboo, R. and Tropea, C., *"Normal impact of a liquid drop on a dry surface: Model for spreading and receding",* Proceedings: Mathematical, Physical and Engineering Sciences, Vol. 458, No. 2022, pp. 1411-1430, 2002.

24. Levin, Z. and Hobbs, P.V., *"Splashing of water drops on solid and wetted surfaces: Hydrodynamics and charge separation",* Philosophical transactions of the Royal Society of London, Series A, Mathematical and Philosophical Sciences, Vol. 269, No. 1200, pp. 222-585, 1971

25. Mundo, CHR., Sommerfeld, M., and Tropea, C., *"Droplet-wall collisions: Experimental studies of the deformation and break-up process",* International Journal of Multiphase Flow, Vol. 21, No. 2, pp. 151-173, 1995

26. Cossali, G.E., Coghe, A. and Marengo, M., *"The impact of a single drop on a wetted surface",* Experiments in Fluids 22, pp. 463-472, 1994

27. Range, K. and Feuillebois, F., *"Influence of surface roughness on liquid drop impact",* Journal of colloidal and interface science 203, pp 16-30, 1998

28. Vander Wal, R.L., Berger, G.M., and Mozes, S.D., *"The splash/non-splash boundary upon a dry surface and thin fluid film",* Experiments in Fluids 40, pp. 53-59, 2006

29. Xu, L., *"Liquid splashing on smooth, rough and textured surfaces",* The American Physical Society, Physical Review E 75, 2007

30. Yoon, S.S., Jepsen, R.A, Demosthenous, B., *"Effects of air on splashing during a large droplet impact: Experimental and numerical investigations",* Atomization and Sprays, Vol. 16, No. 8, pp. 981-996, 2006

31. Rein, M. and Deplanque, J.P., *"The role of air entrainment on the outcome of drop impact on a solid surface"*, Acta Mech. 201, pp. 105-118, 2008

32. Allen, R.F., *"The role of surface tension in splashing",* Journal of Colloid Interface Science 51, 1975

33. Thoroddsen, S.T. and Sakakibara, J., *"Evolution of the fingering pattern of an impacting drop",* Physics of Fluids, American institute of Physics, Vol. 10, No. 6 (June 1998)

34. Asai, A., Shioya, M., Hirasawa, S., and Okazaki, T., *"Impact of an ink drop on paper",* Journal of Imaging Science and Technology, Vol. 31, No. 2, pp. 205-207, 1993

35. Dittmar, D., Fredenhagen, A., Oei, S.B., and Eggers, R., *"Interfacial tensions of ethanol-carbon dioxide and ethanol-nitrogen. Dependence of the interfacial tension on the fluid density- prerequisites and physical reasoning",* Chemical Engineering Science 58 (2003)

36. De Gennes, P.G., *"Wetting: statics and dynamics",* The American Physical Society, Reviews of Modern Physics, Vol. 57, No. 3, Part 1, July 1985

37. Marmanis, H. and Thoroddsen, H.T., *"Scaling of the fingering pattern of an impacting drop",* American Institute of physics, Physics of Fluids 8(6), 1996

38. Purvis, R. and Smith, F.T., *"Air-water interactions near droplet impact"*, European Journal of Applied Mathematics, Vol. 15, pp. 853-871, 2004

39. Rafai, S., Bonn, D., and Boudaoud, A., *"Spreading of non-Newtonian fluids on hydrophilic surfaces",* Journal of Fluid Mechanics, Vol. 513, pp. 77-85, 2004

40. Crooks, R., Cooper-Whitez, J., and Boger, D.V., *"The role of dynamic surface tension and elasticity on the dynamics of drop impact",* Chemical Engineering Science, Vol. 56, pp. 5575-5592 (2001)

41. Betelu, S.I. and Fontelos, M.A., *"Capillarity Driven Spreading of Power-Law Fluids"*, Applied Mathematics Letters 16 (2003) 1315-1320

42. Rozhkov, A., Prunet-Foch, B., and Vignes-Adler, M., *"Impact of drops of polymer solutions on small targets",* American Institue of Physics, Physics of Fluids, Vol. 15, No. 7, 2003

43. Rozhkov, A., Prunet-Foch, B., and Vignes-Adler, M., *"Dynamics and disintegration of drops of polymeric liquids",* Journal of non-Newtonian Fluid Mechanics, Vol. 134, pp. 44-55, 2006

44. Tanner, L.H., *"The spreading of silicone oil drops on horizontal surfaces",* Journal of Physics, D: Applied Physics, Vol. 12, 1979